Montanuniversität Leoben

Influence of Hf on the phase stability and age-hardening behaviour of Ti-Al-N hard coatings

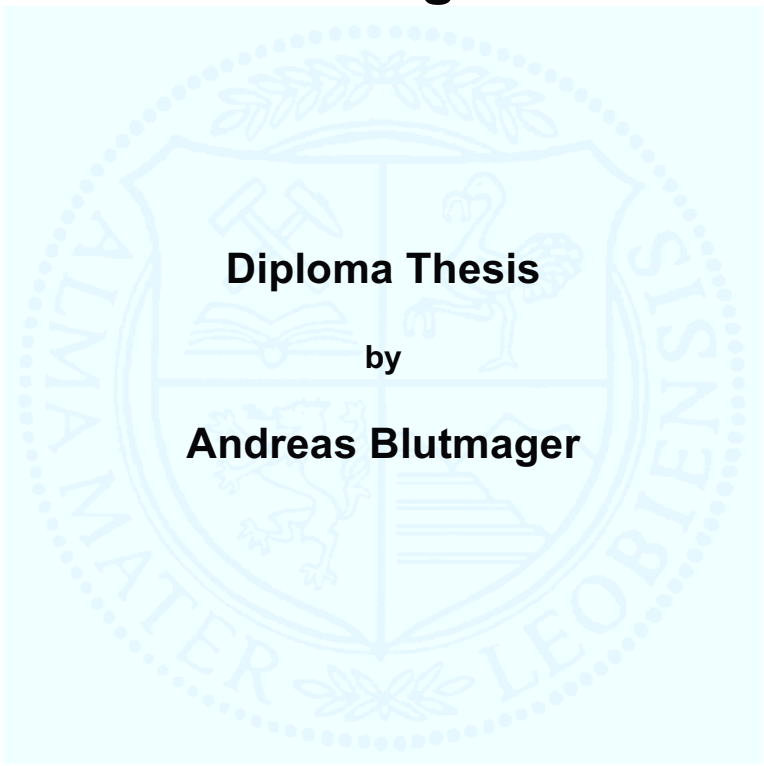

Diploma Thesis

by

Andreas Blutmager

This Diploma Thesis has been carried out at the Department Physical Metallurgy and Materials Testing at the Montanuniversität Leoben (Austria).

Leoben, 1st December 2010

This thesis was funded by the FWF project (Y371) “Atomistic modelling of metastable phases” and provided with the Förderstipendium of the Institute of Mathematics and Statistics at the Montanuniversität Leoben.

Affidavit:
I declare in lieu of ought, that I wrote this thesis and performed the associated research myself, using only literature cited in this volume.

Leoben, 1st December 2010

Acknowledgements

Many people contributed to the production of this diploma thesis and therefore I would like to use this opportunity to express my gratitude to them.

At first, I want to thank **Assoz.-Prof. DI Dr. Paul Mayrhofer** who allowed me to work in his group, of the Department Physical Metallurgy and Materials Testing, and thus be part of his team while I was working on my thesis. Furthermore, he helped me a lot with his great competence in his research field and additionally, he did an amazing job in correcting this diploma thesis.

Another person I really owe my gratitude to is **DI Richard Rachbauer** who has always been willing to respond to my numerous questions in spite of his own time-pressure. During the time I worked at the institute, he has always helped me with some good piece of advice as far as my paper is concerned but, apart from that, we also enjoyed some heated discussions that were definitely not work-related while drinking one or two glasses of beer. Rich, your input and your criticism has always been motivating and making me progress.

Furthermore, I would like to thank **DI Dr. Jörg Paulitsch** who transformed my bad “Burgenland/HTL” English into acceptable scientific and academic writing. No matter which question I asked him, he always tried to find a solution to my problems, even if they were not concerning my research.

I am also very grateful to **Ing. Hannes Pölzl** who was really enthusiastic and such a helping hand that he even sometimes spent additional time at the institute in order to keep the machines running.

I also would like to express my gratitude as well to **DI Robert Hollerweger**, **DI Manfred Schlögl** and **Dr. David Holec**, who are supposed to represent the whole thin film group, for our various interesting discussions, for their hints concerning my work, our delightful lunch breaks and numerous glasses of beer after the workday was over.

I am particularly obliged to my friends, first and foremost **DI Bernd Christian Schrittesser** who helped and supported me in any imaginable way, especially at the beginning of my studies in Leoben. He made sure that the really important activities

in a student's life do not get a raw deal. I have to say that without my friends the time in Leoben wouldn't have been as much fun as it was.

Besonders möchte ich mich bei meiner **Familie** bedanken, die mir diesen Weg ermöglicht hat und abseits des Studiums und der Universität immer für mich da war und mich unterstützt hat.

Last but not least, I would like to express a very special thank to my girlfriend **Petra Rauchbauer**. Without her, I would have certainly stopped studying and left Leoben already a couple of years ago, or wouldn't have finished my studies in the near future. Additionally, I want to thank her for her corrections of this diploma thesis, sometimes until late in the night. Thank you for your mental support during hard times and that you are the person that makes my life complete and valuable.

Abstract

Ti-Al-N based hard coatings are used for a variety of industrial applications due to their outstanding mechanical properties, thermal stability and oxidation resistance. The ever-growing industrial demand for improved properties drives research towards the development of quaternary or even multinary materials. This work focuses on the investigation of Hf-addition to Ti-Al-N. Ti-Al-Hf-N coatings with different chemical composition were prepared by magnetically-unbalanced magnetron sputtering of powder metallurgically prepared Ti-Al-Hf targets (Al/Ti atomic ratio of 2 and Hf contents of 2, 5 and 10 at%, 75 mm diameter and 5 mm thickness) in a mixed Ar-N_2 glow discharge using a substrate temperature of 500 °C. To further vary the chemical composition of the deposited nitride films (in addition to the mentioned target variation) up to eight Ti platelets (5 mm diameter and 3 mm thick) where added at the race-track of the target. Thereby, the chemical composition of the metal-sublattice of the stoichiometric nitride films could be adjusted to values between the following ranges: 27-44 at% Ti, 48-71 at% Al, and 2-9 at% Hf. Investigations by X-ray diffraction (XRD) exhibit a single phase cubic (c, NaCl-type, B1) structure for the coatings with ~2 at% Hf up to Al contents of ~60 at%, with ~5 at% Hf up to Al contents of ~57 at% and with ~9 at% Hf up to Al contents of ~55 at% (the given values refer to the metal sublattice). For higher Al contents the metastable hexagonal close packed wurtzite (w, ZnS-type, B4) phase is favored. Annealing investigations (in vacuum) of the single phase cubic coatings $Ti_{0.381}Al_{0.602}Hf_{0.017}N$, $Ti_{0.386}Al_{0.566}Hf_{0.048}N$ and $Ti_{0.350}Al_{0.555}Hf_{0.095}N$, hence, with a chemical composition close to the transition from cubic to wurtzite phase, exhibit a spinodal-like decomposition of their supersaturated cubic phase to form Al-rich and Ti-rich cubic domains. Up to annealing temperatures of 900 °C no wurtzite like AlN can be detected (by XRD) for all coatings investigated. Whereas the low Hf containing film, $Ti_{0.381}Al_{0.602}Hf_{0.017}N$, exhibits w-AlN after annealing at 1000 °C no w-AlN is present for the higher Hf containing films even up to annealing temperatures of 1200 °C. After annealing at 1400 °C the coatings consist of w-AlN and a solid solution c-Ti-Hf-N, no separate HfN phase could be detected by XRD. The lattice parameters of the obtained cubic solid solution $Ti_{0.96}Hf_{0.04}N$, $Ti_{0.89}Hf_{0.11}N$ and $Ti_{0.79}Hf_{0.21}N$ phases are 4.26, 4.29 and 4.31Å. The hardness evolution, with annealing temperature, of these Ti-Al-Hf-N coatings is in perfect agreement to their structural evolution. All coatings investigated exhibit an age hardening behavior for annealing temperatures above 700 °C, where the formation of cubic Al-rich and Ti-rich domains is dominant. The low Hf-containing film, $Ti_{0.381}Al_{0.602}Hf_{0.017}N$, exhibits a pronounced hardness reduction (from the peak hardness of ~41 GPa at 900 °C to ~34 GPa at 1000 °C) if annealed at

1000 °C or higher, as here the formation of w-AlN starts. The higher Hf-containing films, $Ti_{0.386}Al_{0.566}Hf_{0.048}N$ and $Ti_{0.350}Al_{0.555}Hf_{0.095}N$, exhibit their peak hardness of ~43 and 44 GPa at 900 and 1000 °C, respectively. Even after annealing at 1100 °C their hardness is at the high level of ~38 GPa, as for both films no w-AlN can be detected even up to annealing temperatures of 1200 °C. The results obtained clearly demonstrate that Hf-addition to Ti-Al-N coatings not just increase their hardness from ~30 to 36 GPa in the as deposited state but also increases their thermal stability, as the formation of w-AlN is shifted to higher temperatures.

Kurzfassung

Hartstoffschichten auf der Basis von Ti-Al-N werden aufgrund ihrer außergewöhnlichen mechanischen Eigenschaften, ihrer thermischen Stabilität und Oxidationsbeständigkeit für eine Vielzahl an Industrieanwendungen verwendet. Durch die ständig wachsende Forderung nach verbesserten Eigenschaften, ist es notwendig weitere Forschungsarbeiten in Richtung quaternären und multinären Materialien durchzuführen. Diese Arbeit konzentriert sich auf Untersuchung von Hf-legierten Ti-Al-N Hartstoffschichten. Ti-Al-Hf-N Schichten, mit unterschiedlicher chemischer Zusammensetzung, wurden mittels Magentron Sputtern in einer Ar+N_2 Glimmentladung und einer Substrattemperatur von ca. 500°C hergestellt. Die verwendeten Targets wurden pulvermetallurgisch hergestellten und hatten ein Al/Ti atomares Verhältnis von 2 und verschiedene Hf-Gehalte von 2, 5 und 10 at% (75 mm Durchmesser und 5 mm Dicke). Für eine weitere Variation der chemischen Zusammensetzung wurden, abhängig vom verwendeten Target, bis zu 8 Ti – Plättchen (5 mm Durchmesser und ca. 3 mm Dicke) auf den Sputtergraben des verwendeten Targets gelegt. Dadurch konnte die chemische Zusammensetzung des metallischen Untergitters der stöchiometrischen Nitrid-Schichten innerhalb der folgenden Bereiche variiert werden: 27-44 at% Ti, 48-71 at% Al and 2-9 at% Hf. Untersuchungen mittels Röntgenbeugung (XRD) zeigten eine einphasige kubische (c, NaCl-Typ, B1) Struktur für die Schichten mit ~2 at% Hf bis zu Al Gehalten von ~60 at%, mit ~5 at% Hf bis zu Al Gehalten von ~57 at% und mit ~9 at% Hf bis zu einem Al Gehalt von ~55 at% (diese Werte beziehen sich auf das metallische Untergitter). Für höhere Al Gehalte wird die hexagonal dicht gepackte Wurtzite (w, ZnS-Typ, B4) Phase bevorzugt. Wärmebehandlungen (im Vakuum) der einphasigen, kubischen Schichten $Ti_{0.381}Al_{0.602}Hf_{0.017}N$, $Ti_{0.386}Al_{0.566}Hf_{0.048}N$ und $Ti_{0.350}Al_{0.555}Hf_{0.095}N$, mit einer chemischen Zusammensetzung nahe dem kubisch-hexagonalen Phasenübergang, zeigen eine spinodale Entmischung ihrer übersättigten kubischen Phase in Richtung Al reicher und Ti reicher kubischer Domänen. Bis zu einer Glühtemperatur von 900 °C konnte in keiner Schicht eine Wurtzite-ähnliche AlN Phase detektiert werden (mittels XRD). Die Schicht mit wenig Hf, $Ti_{0.381}Al_{0.602}Hf_{0.017}N$, weist bereits bei einer Glühtemperatur von 1000 °C die Bildung von w-AlN auf. Hingegen kommt es bei den Schichten mit höheren Hf Gehalten erst über 1200 °C zu einer w-AlN Bildung. Nach dem Glühen bei 1400°C bestehen die Schichten aus den beiden Phasen w-AlN und c-Ti-Hf-N. Es konnte mittels XRD keine eigne HfN Phase detektiert werden. Die Gitterparameter der erhaltenen kubischen Mischkristalle $Ti_{0.96}Hf_{0.04}N$, $Ti_{0.89}Hf_{0.11}N$ und $Ti_{0.79}Hf_{0.21}N$ sind 4.26, 4.29 und 4.31 Å. Die Härteentwicklung der Ti-Al-Hf-N Schichten, mit der Glühtemperatur, zeigen eine perfekte Übereinstimmung mit ihrer

Strukturentwicklung. Alle untersuchten Schichten weisen eine Aushärtung durch Glühen über 700 °C auf, solange die kubischen Al-reichen und Ti-reichen Bereiche dominieren. Die Schicht mit wenig Hf, $Ti_{0.381}Al_{0.602}Hf_{0.017}N$, zeigt eine deutliche Härtereduktion (von der höchsten Härte von ~41 GPa bei 900 °C bis ~34 GPa bei 1000 °C) wenn sie über 1000 °C geglüht wird. Bei dieser Temperatur kommt es auch zur Bildung der hexagonal w-AlN Phase. Die Schichten mit höheren Hf Gehalt, $Ti_{0.386}Al_{0.566}Hf_{0.048}N$ und $Ti_{0.350}Al_{0.555}Hf_{0.095}N$, zeigen ihre höchsten Härtewerte mit ~43 GPa bei 900 °C, bzw. mit ~44 GPa bei 1000 °C. Nach dem Glühen bei 1100 °C liegt der Härtewert beider Schichten immer noch bei ~38 GPa, da es bei diesen Schichten bis zu 1200 °C zu keiner hexagonalen w-AlN Ausscheidung kommt. Die Ergebnisse zeigten eindeutig, dass die Zugabe von Hf zu Ti-Al-N Hartstoffschichten, nicht nur deren Härte steigert, von ~30 bis ~36 GPa, sondern auch deren thermische Stabilität verbessert. Die Ausscheidung von der hexagonalen w-AlN Phase wird mit steigendem Hf Gehalt zu höheren Temperaturen verschoben.

Table of contents

Table of figures

Table of captions

Table of abbreviations and used symbols

a	Lattice parameter
Ar^+	Argon ion
c	Cubic structure
d	Lattice plane distance
h, k, l	Mitter indizes
n	Count
PVD	Physical vapour deposition
SZM	Structure zone model
T_a	Annealing temperature
UBM	Unbalanced magnetron sputtering
w	Wurtzite structure
XRD	X-ray diffraction analysis
θ	Scattering angle
λ	Wavelength

1 Introduction

"Thin-film technology is one of the oldest arts and one of the newest sciences" [1].

Fire gildig coating, which has already been used by the Egyptians, is a process by which Amalgan is spread on metallic objects and then annealed and furthermore, it is one out of numerous finishing and finally coating processes. These processes have already contributed to the improvement of materials in ancient times. During that time in history, the improvement, finishing and corrosive protection were most important.

Soon, it was discovered that these layers and coatings do not only influence the appearance of these objects but other characteristics can be improved as well by using adapted coatings. This is the reason why coatings with the following properties have been developed: wear resistance, corrosion resistance and increasing hardness. Examples for the application of these developed coatings are cutting tools, e.g. drillers, turning tools, cutters and so on.

One of the discovered coatings was Ti-N which caused a radical improvement of these properties but also the disadvantage of thermal stability. A further improvement was achieved by adding Al to this Ti-N coatings. In order to enhance the bonification of these coatings, further elements such as Y, Nb, B, Zr etc. were added [2].

In this thesis the element Hf is chosen to investigate its influence on the structure development and properties of Ti-Al-N coatings, whereby the focus was on the growth of cubic stabilized coatings, which was achieved by adjusting the Ti content of the targets. Hafnium is known to improve the oxidation resistance of Ti-Al alloys, where best results can be obtained, by adding around 0.24 at%. For higher amounts of Hf, the positive effect decreases. The main focus is on hardness and thermal stability of Ti-Al-Hf-N coatings. In order to verify the effects and developments with increasing Hf content and increasing temperature, a sum of investigations were done and the results are posed and discussed in the following pages [3].

2 Film deposition

2.1 Introduction

The material's surface and its properties are of great importance, because they directly affect the fields of application and are the immediate connection to another surface or their environment.

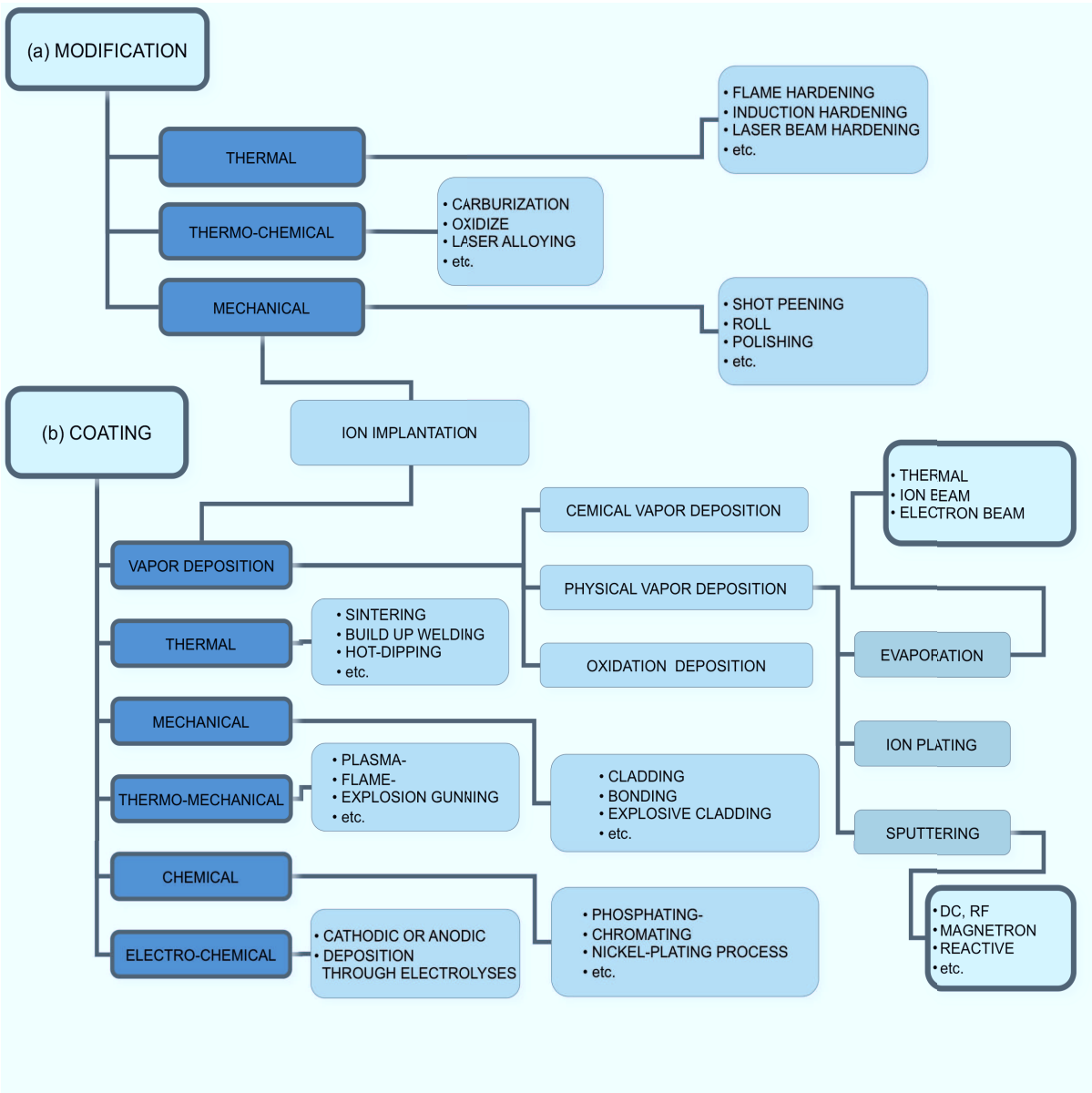

Figure 2.1: Overview of surface modifications (a) and coating processes (b) [4, 5, 6].

Therefore, a lot of different techniques have been investigated to modify the material's surface and surface near regions, as well as to deposit thin films [4]. Figures 2.1a and b, summarize the most important techniques for surface modifications and thin film depositions, respectively.
There are numerous schemes to classify coating processes, as their individual categorization is somehow difficult as many of them can count for different categories. The arrangement in detail depends on the general headings such as in wetting processes, chemical processes, spraying processes, conduction and diffusion processes. Also the separations towards the medium, the substrate and so on can be possible [4].

The main focus in this work will be on film deposition using the physical vapour deposition (PVD) technique, and here especially on sputtering. Therefore, the main principles are summarized in the following chapters.

2.2 Physical vapour deposition (PVD)

PVD techniques can be divided into three processes, sputtering, evaporation and ion plating. Nevertheless, for industrial applications the most common processes are arc evaporation and sputtering. The main advantages of PVD coatings are the variety of substrate materials, which can be used, e.g. metals, alloys, ceramics, plastics as well as the wide range of possible coatings that can be prepared, such as nitrides, carbides, oxides and borides [5, 6].

2.2.1 Unbalanced magnetron sputtering

Sputtering is based on the bombardment of a solid source material, usually named as target, by ions, mainly Ar^+, which eject species out of the target surface. These ions are created by a glow discharge between the target (cathode) and the substrate or chamber walls (anode). To obtain sufficient energy for sputtering events, the Ar^+ ions are accelerated by a negative electric field, a negative potential applied to the target, cathode (see Fig. 2.2a). Thereby, the Ar^+ ions bombarding the target surface will cause collision cascades in the surface near regions, which can lead to the ejection of neutral or charged species, as schematically illustrated in Fig. 2.2b.

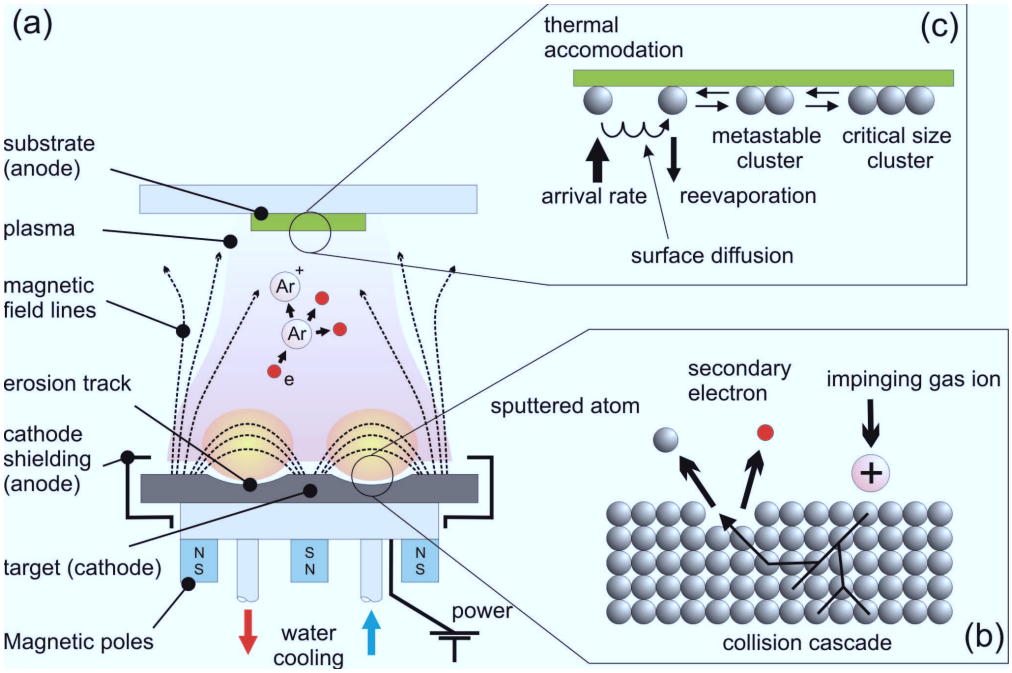

Figure 2.2: Schematically magnetron sputtering prozess [7].

The sputtered species leave the target with certain energy and traverse the plasma to the substrate. On the substrate surface, the arriving species can either re-evaporate or form clusters by nucleation and start the film growth, as schematically presented in Fig. 2.2c. A magnetic arrangement behind the target, as shown in Fig. 2.2a, enhances the Ar^+ ion density close to the target, which allows sputtering at lower gas pressures and therefore reduces collision events of the sputtered species on their way to the substrate. Hence, the sputtering rate increases. [1, 4, 6, 7, 8, 9, 10, 11, 12]. The unbalanced magnetron (UBM) sputtering system used in this thesis, which allows also for an enhanced Ar^+ density close to the substrate, as not all charge carriers (like electron and Ar^+ ion) are trapped to the target, is beneficial for the thin film growth, as these charge carriers can be used to stimulate nucleation and growth processes by applying a bias potential to the substrate [13, 14, 15, 16].

2.2.2 Thin film nucleation and growth

Sputtered species, either charged or neutral, can absorb on the substrate surface. These will partially resorb or form metastable or even stable clusters, which will grow continuously, if the adsorption rate over counts the desorption rate, see Fig. 2.2.c. Ongoing diffusion processes will further lead to the formation of islands and finally the thin film. There are three different idealized models, which describe the mechanisms of thin film growth, which are schematically illustrated in Fig. 2.3.

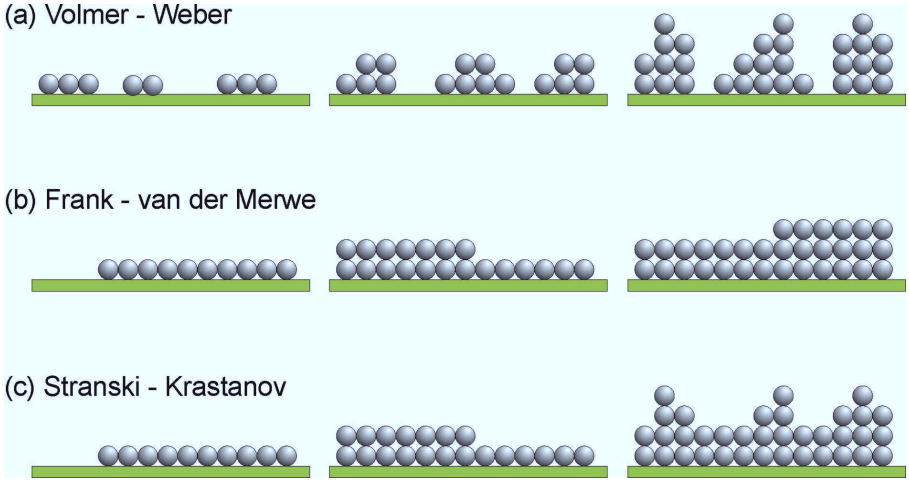

Figure 2.3: Three ways of idealized film growth, (a) Volmer-Weber growth, (b) Frank van der Merwe growth and (c) Stranski-Krastanov growth [7].

Volmer-Weber growth (*island growth, Fig. 2.3a*) takes place when the affinity between the ad-atoms is higher than the affinity to the substrate surface. Otherwise,

the *Frank van der Merwe growth* (*layer by layer growth, Fig. 2.3b*) is the preferred grow mechanism. The *Stranski-Krastanov growth* can be describe as a mixture of island and layer by layer growth (Fig. 2.3c), depending on the changing film and substrate surface energies during film growth. The morphology and microstructure of the forming thin film can be influenced by the mobility of the ad-atoms and surface and bulk-diffusion which strongly depend on the temperature and the energetic bombardement by various species which can transfer their energy to the film forming species. [1, 10, 11]. The resulting microstructure can be described in structure zone models (SZM), which show the film growth in relation to e.g., temperature, bias potential and working gas pressure [17, 18]. Figure 2.4 shows such a possible SZM including some illustrated features from the Thornton diagram and some addition of potential and kinetic energy effects of particles, which arrived on the surface.
For further details, please see [19].

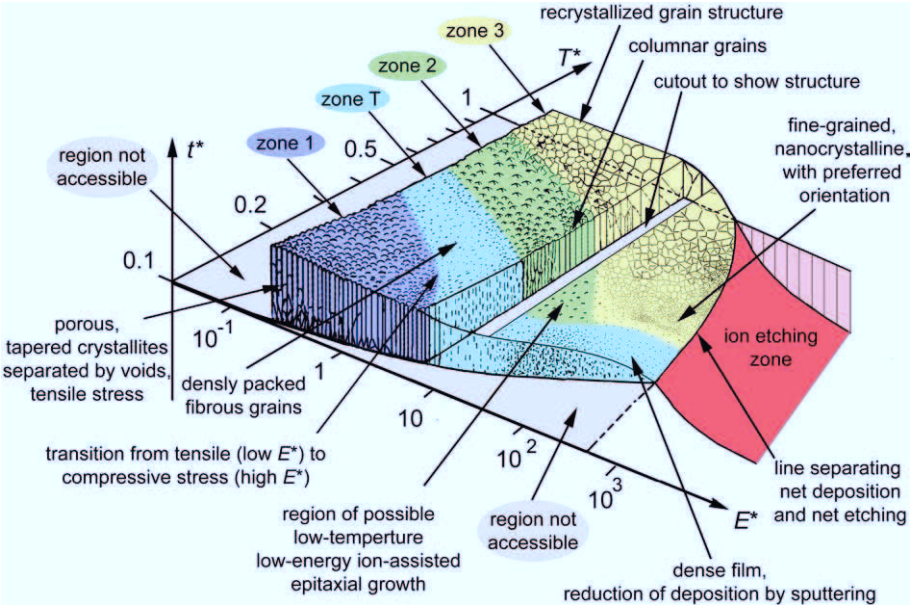

Figure 2.4: Structure zone model by A. Anders [19]

3 Coating system

Coatings from the Ti-Al-N system are heavily used in industry due to their excellent properties, like high hardness, wear resistance, corrosion and oxidation resistance [20, 21, 22, 23, 24].

3.1 Ti-Al-N

Figure 3.1 shows a section of the Ti-Al-N pseudo-phase diagram, including the simplified TiN-AlN quasi-binary system for plasma assisted vapor deposition techniques. The face centered cubic structured (NaCl-typ, B1) $Ti_{1-x}Al_xN$, most important for the tooling industry, is accessible depending on the growth conditions up to ~ 60-70 mol% of AlN. The gap between the cubic and the hexagonal phase (ZnS-type, B4, wutzite) increases with higher growth temperature approaching the equilibrium conditions, where the solid solubility of TiN and AlN is extremely limited, consequently the miscibility gap between TiN and AlN is rather high. The broad single-phase fields for deposition temperatures below ~ 700 °C (Fig. 3.1), show that the material conditions obtained by plasma assisted vapor deposition techniques can be far away from equilibrium. Consequently, the obtained supersaturated phases can occupy a high chemical driving force for decomposition into their stable components [25].

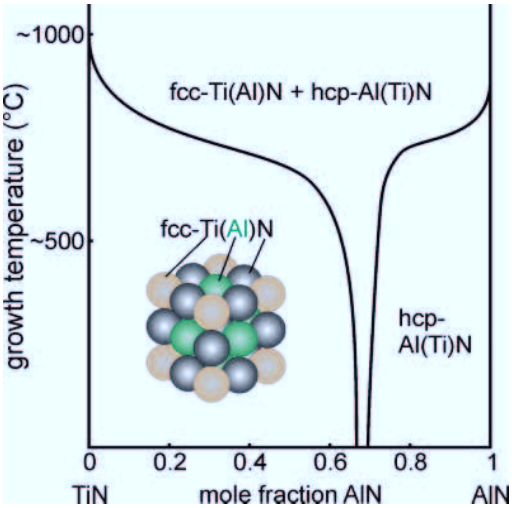

Figure 3.1: PVD-pseudo-phase diagram of the quasibinary section of TiN-AlN [25].

$Ti_{1-x}Al_xN$ coatings, which are known for their excellent wear resistance, used in applications of high speed and dry cutting show, in the as-deposited state, a supersaturated solid solution with NaCl-type structure. Figure 3.2 shows the hardness over the annealing temperature, where the hardness increases between 600 and 950 °C, indicating age hardening effects. The three different phases after annealing at T_a = 1030 °C are: c-$Ti_{1-x}Al_xN$ (matrix), c-TiN and c-AlN. The AlN domains, which are mostly formed by spinodal decomposition (at T_a ~ 700 °C), coarsen with increasing temperature. Connected with the formation of AlN-rich domains is also the formation of TiN-rich areas. At temperatures above 900°C, which increases also the peak hardness, also the wurtzite-type AlN phase can be detected. With further increasing T_a the phase fraction of w-AlN increases which causes the hardness to decrease. The decomposition process is complete after annealing at T_a = 1400 °C where the c-AlN phase completely transformed into its stable w-structure [25, 26, 27, 28].

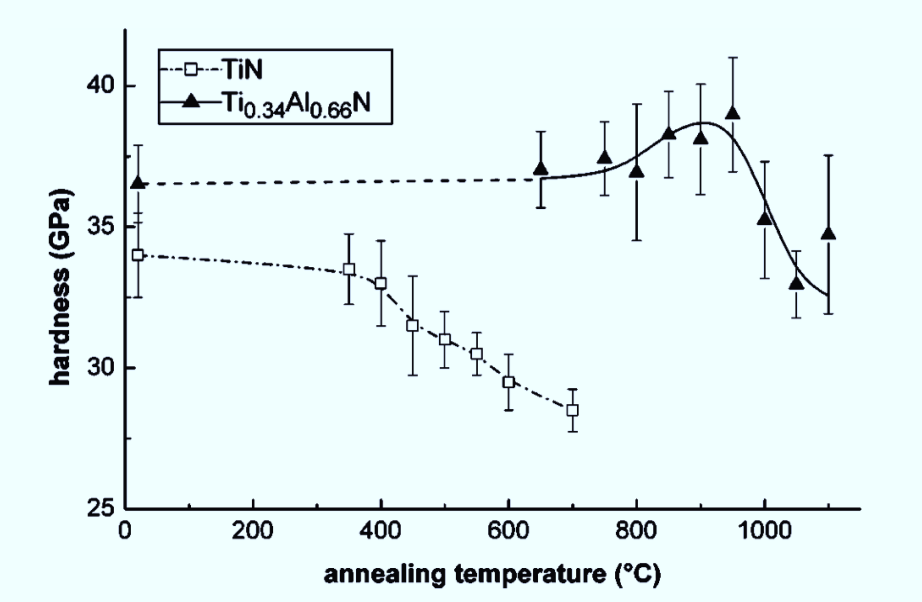

Figure 3.2: Hardness over annealing temperature [26].

Figure 3.3 indicates the structural change from the NaCl-type to the ZnS-type, cubic and hexagonal, respectively, as well as the resulting hardness values for $Ti_{1-x}Al_xN$. Such a change also affects the microstructure and the morphology of these coating. PalDey S. et al., described a transition from fibrous to columnar structure at Al contents around 60% and higher [3, 29, 30].

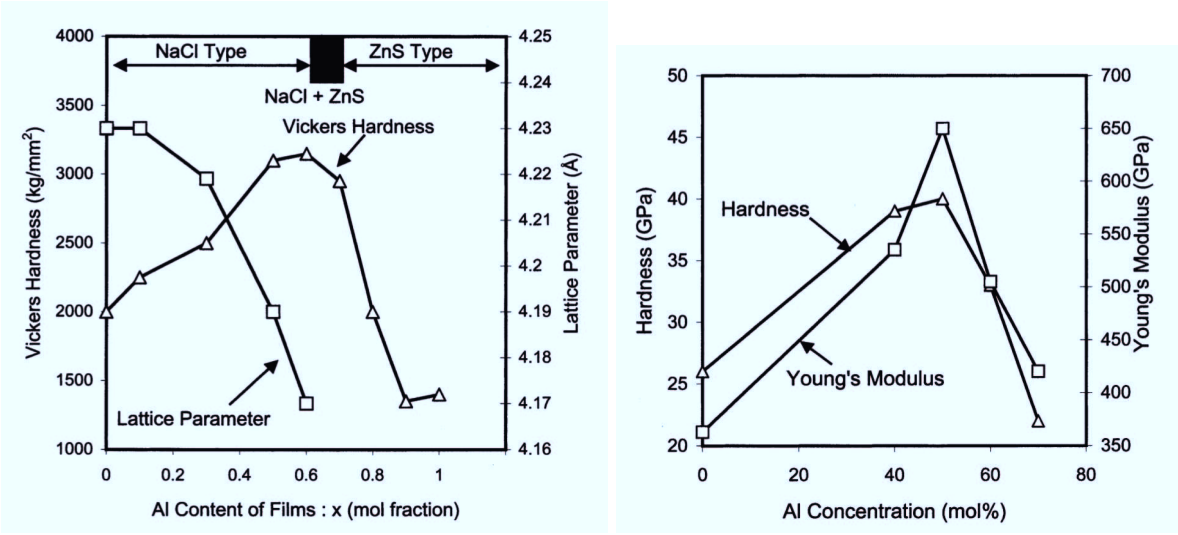

Figure 3.3: On the left handside, the lattice parameters and microhardness values as a function of the Al content in $Ti_{1-x}Al_xN$ films and on the right handside, the hardness compared with the young's modulus as a function of the Al content [29]

3.2 Addition of Hafnium

Numerous research groups have already shown, that the properties of Ti-Al-N coatings, can be significantly modified by alloying with various elements, like Nb, Cr, B, Zr, Y or Hf to form a quaternary alloy Ti-Al-X-N [2]. Manfred Pock [31] compared Ti-Al-X-N quaternary alloys containing X = Hf, Nb and T_a in his work, whereby in this thesis the focus was on the growth of cubic stabilized coatings, which was achieved by adjusting the Ti content of the targets. In this thesis the focus was on alloying Hf to the Ti-Al-N. Hafnium is known to improve the oxidation resistance of Ti-Al alloys, where best results can be obtained, by adding around 0.24 at%. For higher amounts of Hf, the positive effect decreases [31, 32]. Furthermore, Hf improves the mechanical properties, the high temperature strength, the ductility as well as the creep resistance, for details see [33]. The addition of Hf to the Nb-15W-0.5Si-2B alloy increases its hardness up to 1400°C by the solid-solution effect and increases its yield stress up to 365 MPa, as compared to 180 MPa of a Hf-free alloy [34].

4 Experimental

This chapter only briefly introduces the used deposition and investigation techniques. For more detailed information see the given references.

4.1 Deposition system

All coatings investigated were deposited with a modified Leybold Heraeus A-400 magnetron-sputtering unit, shown in Fig 4.1. Details are given in [35, 36, 37, 38, 39].

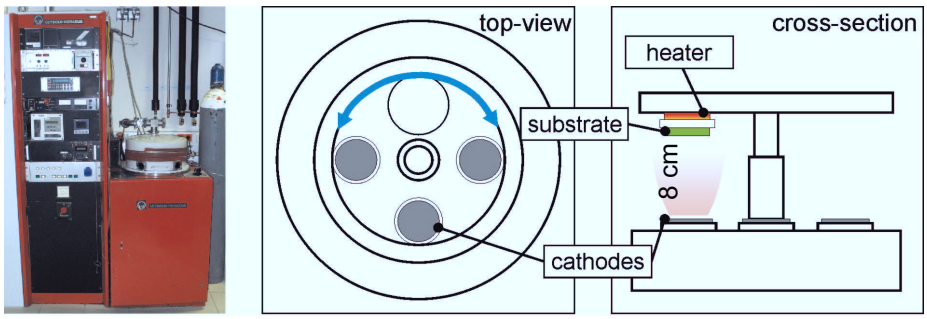

Figure 4.1: Leybold Heraeus A-400 magnetron-sputtering unit with a schematic presentation of the chamber [7].

In general, any deposition was composed of the following steps:

- The substrates were first cleaned in the ultrasonic cleaner for 5 min in acetone and afterwards 5 min in ethanol.
- After cleaning the chamber the substrate were implemented and arranged like shown in Fig. 4.2.
- Then the chamber was evacuated and beaked out.
- Next pre-sputtering of the targets surface follows and also the substrates were Ar^+ ion etched.
- Finally the film deposition was started.

The parameters used for the depositions are given in Tab. 4.1:

Table 4.1: Summary of the parameters used for the depositions.

	Bake out	Pre-sputtering	Etching	Deposition	After deposition
Temperature [°C]	ca. 500	-	ca. 500	ca. 500	-
Pressure [mbar]	ca. $3 \cdot 10^{-5}$	ca. $7 \cdot 10^{-3}$	ca. $1 \cdot 10^{-2}$	ca. $2 \cdot 10^{-3}$	ca. $2 \cdot 10^{-5}$
Time [min]	105	5	10	60, 120 (Powder)	-
Argon [sccm]	-	40	40	9	-
Nitrogen [sccm]	-	-	-	7.9	-
Potential Magnetron [V]	-	ca. 400	-	ca. 460	-
Current Magnetron [A]	-	ca. 1	-	ca. 0.87	-
Power Magnetron [W]	-	400		400	-
Power RF-Generator [W]	-	-	100	-	-
Bias potential [V]	-	-	-	-50	-

-...zero/ not measured/ not needed

The substrates are positioned approximately 8 cm above the target, as indicated in Fig. 4.1. To vary the Ti content of the Ti-Al-Hf targets used, Ti platelets with a purity of 99.9% were regularly placed on the target surface at the sputtering race-track, as indicated in Figs. 4.2a and b. Additionally, the position of the substrates above the target is indicated by the rectangles in Fig. 4.2a. This is important, as a changed configuration would result in significant changes of the chemical composition the coatings and their uniformity. Figure 4.2b indicates the chosen Ti platelets number and position, based on the results of the pre-investigations (see chapter 5.1), for depositing cubic stabilized Ti-Al-Hf-N coating. The position of the substrates is not given here as they cover all positions or the whole sample holder, resulting in a uniform distribution of the substrates.

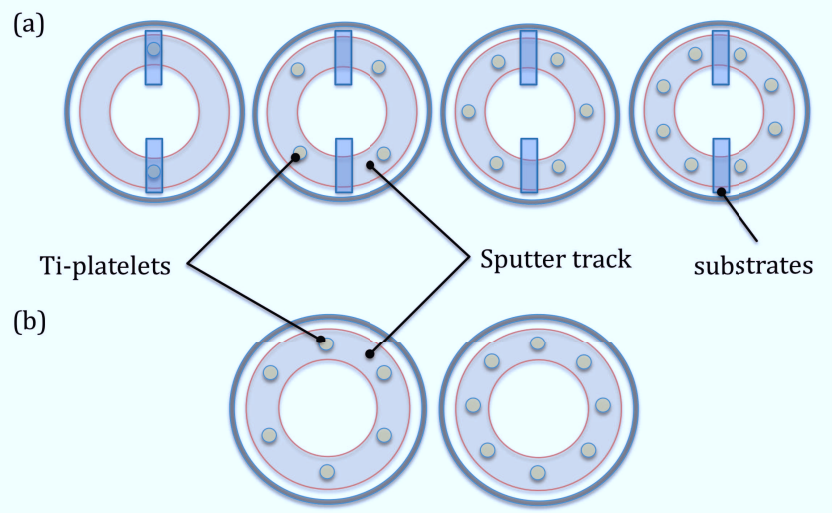

Figure 4.2: Disposal of Ti platelets for the preliminary tests (a) and for the final film deposition (b).

Table 4.2 gives the chemical composition of the targets used (Plansee AG) and the number of Ti platelets for the individual targets for the final deposition runs.

Table 4.2: Targets used and number of other Ti platelets (5 mm in diameter) for the individual targets to obtain cubic stabilized Ti-Al-Hf-N coatings, see chapter 5.1.

Targets	Chemical composition [at%]			Number of Ti platelets	Purity [%]
	Ti	Al	Hf		
$Ti_{0.327}Al_{0.653}Hf_{0.02}$	32.7	65.3	2	6	99.9
$Ti_{0.317}Al_{0.633}Hf_{0.05}$	31.7	63.3	5	8	99.9
$Ti_{0.30}Al_{0.60}Hf_{0.10}$	30	60	10	6	99.9

4.2 X-ray diffraction (XRD) analysis

The non-destructive XRD investigation technique is common to obtain structural information of materials. Based on the nature of the X-ray, there will be either a constructive or destructive interference with any ordered lattice. Such interferences generate material specific pattern when monitored. Bragg's law, $n \cdot \lambda = 2 \cdot d \cdot \sin(\Theta)$, gives the precondition for constructive interference. Whereas n is an integer, λ is the wavelength of the X-ray (1.54 Å for CuKα, used in this thesis), d is the lattice plane

spacing and θ designates the scattering angle, as schematically shown in Fig. 4.3. For detailed information on XRD, please see for example [40, 41, 42].

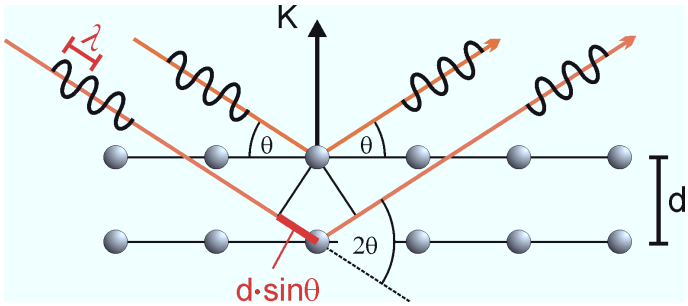

Figure 4.3: Schematical representation of the X-ray diffraction in an atomic lattice [7].

XRD measurements were performed with a Bruker-AXS D8 Advance Diffractometer using the following parameters:

Table 4.3: Parameters for the XRD measurements.

	Steps	Time	Methode	Angle	Source	Detector	Additional data
Coatings on substrates	0.02°	1.2 s	Bragg Brentano	20-85°	CuKα	Sol-X	No rotation
Powdered coating samples	0.02°	1.2 s	Bragg Brentano	20-85°	CuKα	Sol-X	Rotation

4.3 Nanoindentation

Mechanical testing of thin films is not as easy as testing uncoated materials, because there is an influence from the general softer substrate. Nanoindentation is a common technique to minimize the influence from the material under the deposited hard coating. To obtain results, with a minimized influence from the substrate, the penetration depth into the coating should not exceed 10% of the film thickness. The resistance against the penetration of the material is directly connected with the hardness and elastic modulus of thin films. Indentation tests were performed with a definite diamond indenter. Figures 4.4a and b show a scheme of the hardness measurements and the obtained load-displacement curve from which the hardness H and the indentation modulus E of the coatings were obtained. Further details on the

nanoindentation and the evaluation of the obtained load-displacement curves to derive H and E are given in [43, 44, 45].

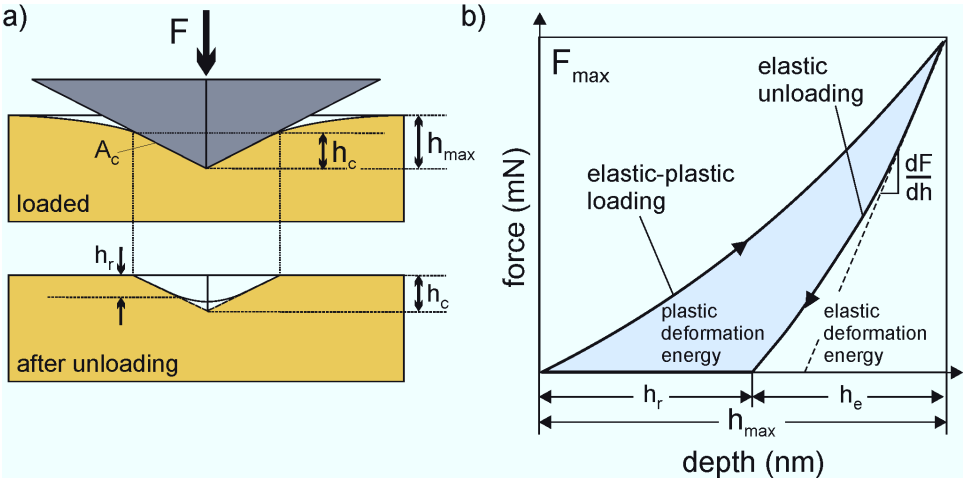

h_{max}.... Total indentations depth measured from specimen free surface
h_r..... Depth of residual impressions
h_e..... Elastic depth of penetration for unloading
h_c..... Depth of the contact indenter - material
A_c..... Contact area under peak load
F..... Force

Figure 4.4: Schematic representation of a nanoindentation (a) and a load-displacement curve (b) [7, 43].

4.4 Vacuum annealing

Vacuum annealing of coated Al_2O_3 (7x21x0.38 mm^3) and powdered coatings (after remaining from their low alloyed steel foil) was conducted in a vacuum furnace (HTM Reetz GmbH – Vakuum - Kaltwandofen) having a base pressure of ≤ $1x10^{-5}$ Pa at the measured temperature of 1400 °C. The powdered coating sample and the coatings on Al_2O_3 were annealed to temperatures T_a of 600 to 1400 °C (in 100 °C steps) with a heating rate of 20 K/min and held at T_a for 1 minute. To minimize further annealing effects during cooling down, the highest possible cooling rate of 50 K/min was used [46].

4.5 Cohen-Wagner method

The Cohen-Wagner method is used to calculate stress free lattice parameters out of a number of XRD peak positions using a linear regression. The Miller indices for the

calculations are taken from the Joint Committee on Powder Diffraction Standards (JCPDS files), and the peak position was measured by hand with the software Origin 8.1. The obtained lattice parameters are plotted against the Cohen-Wagner coefficient ($a=(\cos^2(\theta)/(\sin(\theta))-\cos^2(\theta)/\theta$). The stress-free lattice parameter is received by the value, where the trend line traverses the y-Axis [47].

4.6 Morphology and chemical analyses

The morphology of the coatings was investigated with a scanning electron microscope (SEM), Zeiss SUPRA40VP. The chemical composition was measured with energy-dispersive X-ray spectroscopy, attached to this SEM, and is shown for some important coatings in Tab. 5.1. For further information, please see [48].

4.7 Stress measurements

Residual stress is a consequence of inhomogeneous macro- and microscopic elastic and elastic-plastic deformation. These residual stresses are basically measured by the deflection of the fused silica platelets of the preliminary tests.

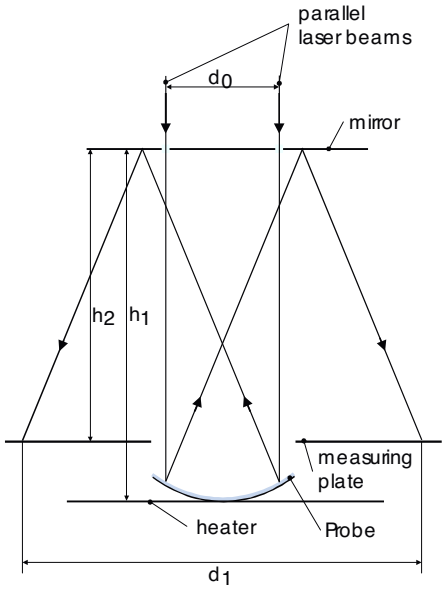

Figure 4.5: Beam path of the used stress measurement system [15].

In this thesis the stress measurements were done only at room temperature. Figure 4.5 shows the principle of the measurement via two parallel laser beams. With

$r=2 \cdot L \cdot d_0 / (d_0 + d_1)$ the radius of the osculating circle can be calculated, L gives the length of the beam path, d_0 and d_1 are the diameters and h_1 and h_2 the high, which are shown in Fig. 4.5 [31].

4.8 Thickness measurements

Figure 4.6 shows a typical calotte, which is used to measure the coatings thickness. The thickness of the coatings was measured using a steel ball and a diamond emulsion as an abrasive medium. Using a light optical microscope and the analysis® software the thickness of the coatings can be evaluated.

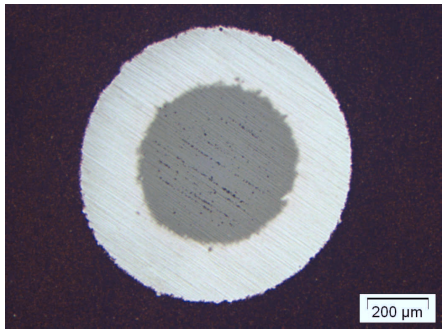

Figure 4.6: Typical calotte for a thickness measurement.

5 Results and discussion

5.1 Structure and chemical composition of Ti-Al-Hf-N coatings

Preliminary tests were conducted to evaluate the chemical composition forming cubic to the hexagonal structure of Ti-Al-Hf-N. Using Ti-Al-Hf targets with a fixed Al/Ti ratio of 2 and ranging Hf contents of 2, 5 and 10 at% varied the Hf content of the films. The Al/Ti ratio of the films was varied by placing Ti platelets, see chapter 4.1, at the race-track. As described by M. Pock [31] and K. Kutschej et al. [2] when using the $Ti_{0.327}Al_{0.65.3}Hf_{0.02}$, $Ti_{0.317}Al_{0.633}Hf_{0.05}$ and $Ti_{30}Al_{60}Hf_{10}$ target with the depositing plant Leybold Heraeus A-400 (also used here) and the given deposition conditions, films are obtained that contain also a wurtzite structure next to the metastable cubic structure. To stabilize the cubic structure Ti platelets were placed at the sputter race-track to increase the overall Ti content as described earlier.

The following chapters summarize the main outcome to determine the chemical composition where the coatings undergo a transition from the metastable cubic structure to the metastable wurtzite structure, when using the three different Ti-Al-Hf target compositions, on the resulting structure using XRD.

5.1.1 Coatings prepared from the target with 2 at% Hf

Figure 5.1 shows the XRD patterns of Ti-Al-Hf-N coatings prepared from the $Ti_{0.327}Al_{0.653}Hf_{0.02}$ target with increasing amount of Ti platelets. The XRD pattern of the coating with the chemical composition $Ti_{0.272}Al_{0.707}Hf_{0.021}N$, (obtained from the target without Ti addition) indicates a predominant wurtzite structure. When adding 2 Ti platelets, the chemical composition of the coating changes to $Ti_{0.299}Al_{0.681}Hf_{0.020}N$. The intensity of the wurtzite reflexes decrease and the cubic ones sharpen and increase in intensity. Addition of 4 Ti platelets results in the formation of $Ti_{0.353}Al_{0.630}Hf_{0.017}N$, where almost no wurtzite reflex can be detected anymore, see Fig. 5.1. For the coating $Ti_{0.371}Al_{0.612}Hf_{0.017}N$, which is obtained from the $Ti_{0.327}Al_{0.653}Hf_{0.02}$ target with 6 Ti platelets, only cubic reflexes can be detected. The sharp XRD peaks at around 32 to 65 degree are from the Si substrate. The increasing Ti/Al ratio, or decreasing Al contents favour the formation of the metastable cubic structure.

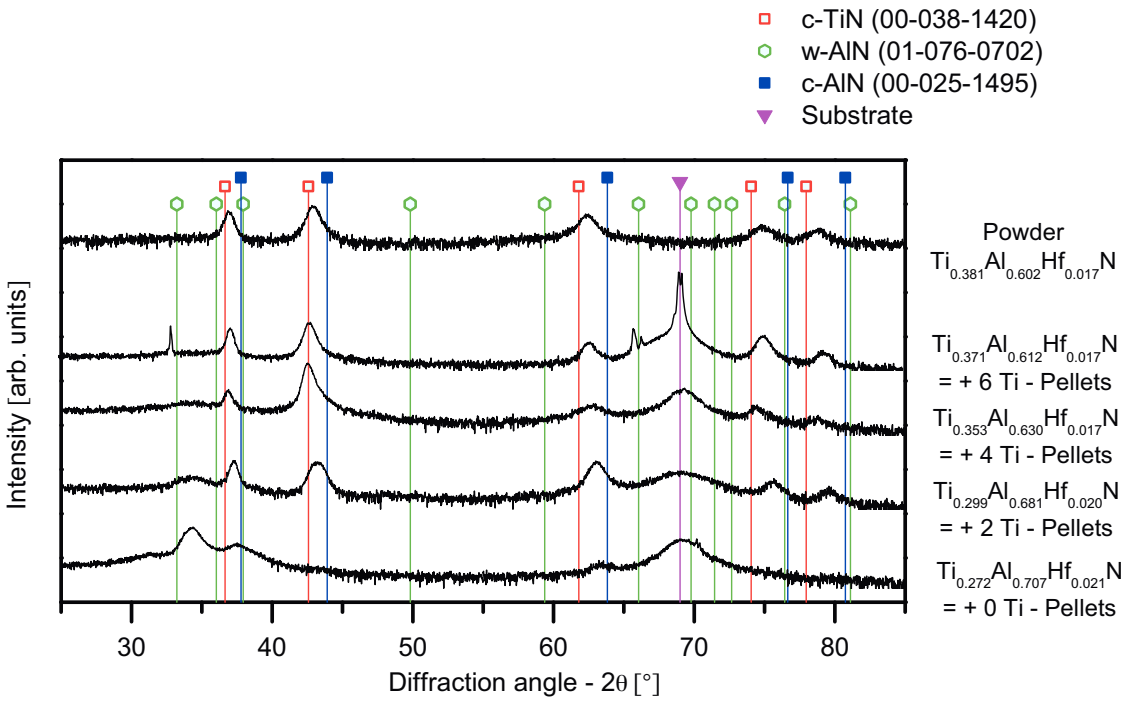

Figure 5.1: XRD patterns of the coatings obtained from the $Ti_{0.327}Al_{0.65.3}Hf_{0.02}$ target with the addition of 0, 2, 4 and 6 Ti platelets.

Based on these results, cubic stabilized coatings, for further studies, are prepared with an addition of 6 Ti platelets on the $Ti_{0.327}Al_{0.653}Hf_{0.02}$target.

5.1.2 Coatings prepared from the target with 5 at% Hf

Figure 5.2 shows XRD patterns of coatings prepared from $Ti_{0.317}Al_{0.633}Hf_{0.05}$ targets with the addition of 0, 2, 4, 6 and 8 Ti platelets. Without adding Ti platelets to the Ti-Al-Hf target the prepared coatings exhibit a chemical composition of $Ti_{0.288}Al_{0.660}Hf_{0.053}N$ and a dominant wurtzite structure, see Fig. 5.2 at the bottom. By adding 2 Ti platelets to the targets race-track, the chemical composition changes to $Ti_{0.323}Al_{0.628}Hf_{0.048}N$ and the intensity of the wurtzite reflexes decreases with a concomitant increase of the cubic reflexes, see Fig. 5.2. A further addition of 2 Ti platelets results in the formation of $Ti_{0.361}Al_{0.595}Hf_{0.045}N$ and a further increase of the cubic XRD reflexes, where still some increased background in the 2θ range of 32 to 36 ° suggests the formation of a wurtzite like phase. With the addition of 6 Ti platelets to the targets race-track the chemical composition further changes to $Ti_{0.351}Al_{0.616}Hf_{0.032}N$ and the cubic reflexes become even more dominant. Nevertheless, as also for this coating the increased background at 32 to 36°

suggests the presence of wurtzite like phases, coatings are prepared from the target with the addition of 8 Ti platelets. This results in the formation of $Ti_{0.386}Al_{0.566}Hf_{0.048}N$ where the XRD investigations suggest a single-phase cubic structure see Fig. 5.2. Thus, in this thesis, the coating $Ti_{0.386}Al_{0.566}Hf_{0.048}N$ is further investigated towards its thermal stability.

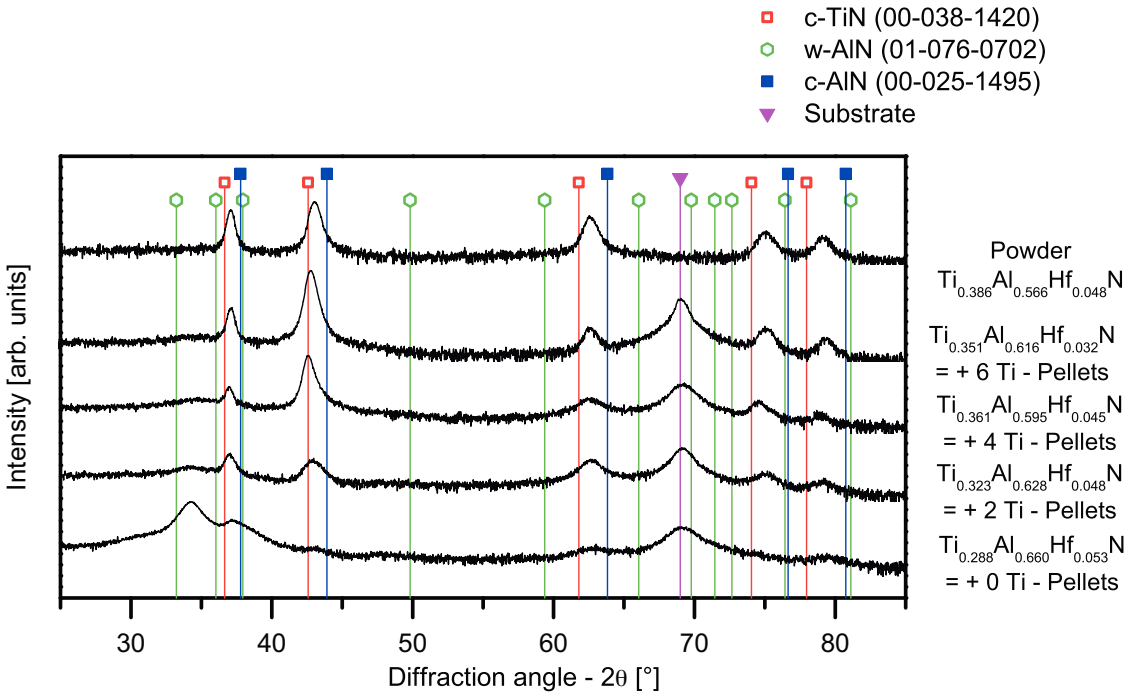

Figure 5.2: XRD patterns of the coatings prepared from the $Ti_{0.317}Al_{0.633}Hf_{0.05}$ target with the addition of 0, 2, 4, 6 and 8 Ti platelets.

5.1.3 Coatings prepared from the target with 10 at% Hf

Figure 5.3 shows the XRD pattern of the coatings sputtered from the $Ti_{0.30}Al_{0.60}Hf_{0.10}$ target, with the addition of 0 2, 4, 6 and 8 Ti platelets. The coating prepared from the $Ti_{0.30}Al_{0.60}Hf_{0.10}$ target without additional Ti corresponds to $Ti_{0.272}Al_{0.634}Hf_{0.094}N$, and the XRD pattern suggests a nanocrystalline structure with mainly wurtzite like phases, see Fig 5.3. By the addition of two Ti platelets to the target race-track a pronounced change towards the cubic structure is obtained, see Fig. 5.3. With the addition of 4, 6 and 8 Ti platelets the chemical composition changes to $Ti_{0.340}Al_{0.566}Hf_{0.095}N$, $Ti_{0.393}Al_{0.519}Hf_{0.088}N$ and $Ti_{0.440}Al_{0.480}Hf_{0.080}N$, respectively, and no wurtzite like phases can be detected. With increasing Ti, or decreasing Al content the cubic reflexes shift to lower angles suggesting a larger lattice parameter, which is in

perfect agreement with the chemical variation, as the lattice parameter should increase with decreasing Al content.

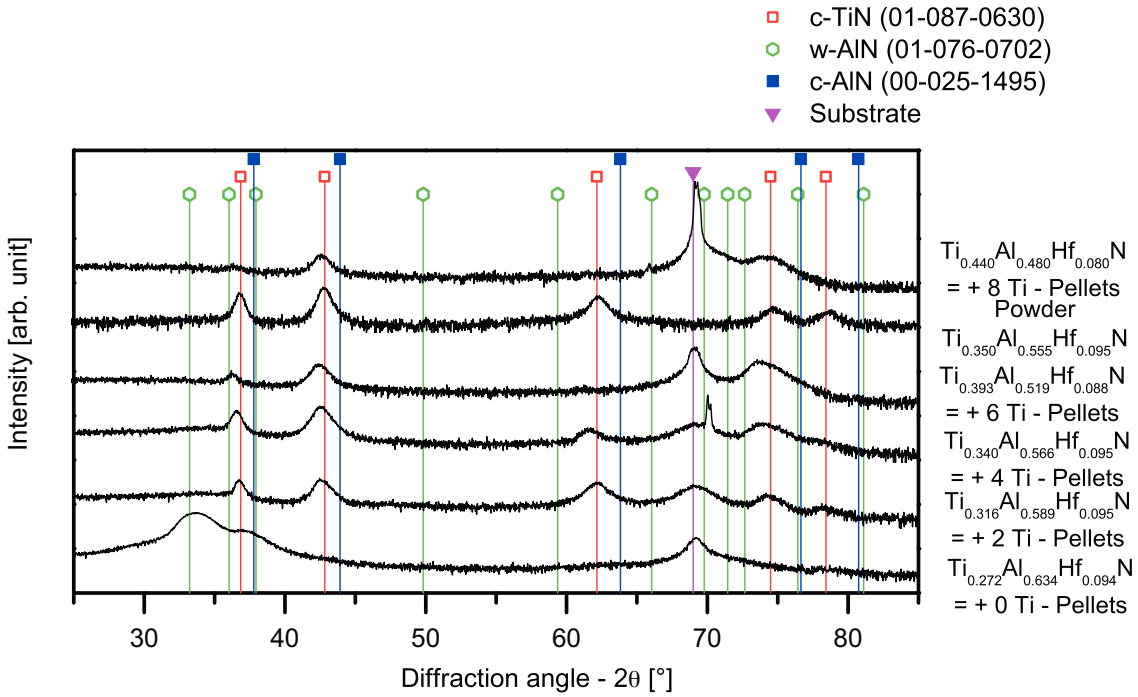

Figure 5.3: XRD patterns of coatings prepared from the $Ti_{0.30}Al_{0.60}Hf_{0.10}$ target with addition of 0, 2, 4, 6 and 8 Ti platelets.

5.1.4 Chemical composition

Figure 5.4 shows the chemical composition of the prepared coatings, which are shown in the quasi-ternary system TiN-AlN-HfN. The marked area in this quasi-ternary system indicates the transition area (from cubic to wurtzite) in which the film-structure is a mixture of the cubic and wutzite one (c+w). Close to the AlN corner of the triangle the structure is pure wurtzite (w) and the TiN and HfN rich sides prefere the cubic structure. The chemical compositions of the coatings are measured with EDX, see chapter 4.6, and placed in the quasi-ternary system.

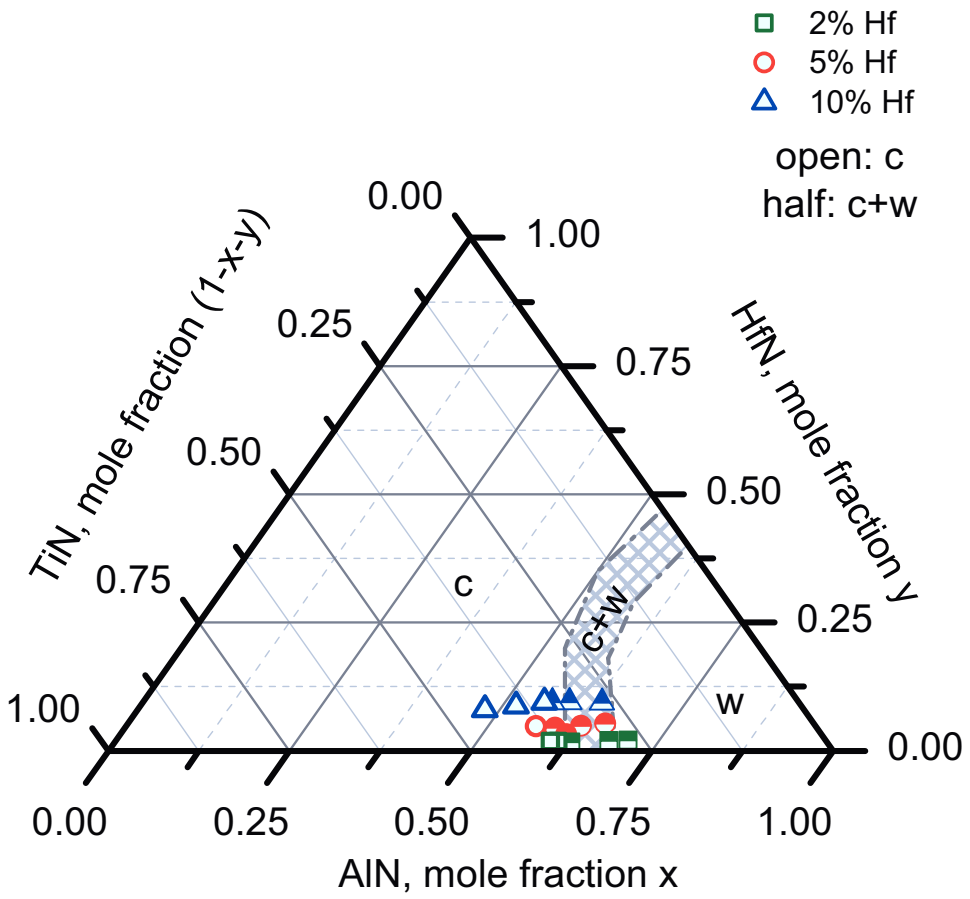

Figure 5.4: Overall chemical composition of the as deposited $Ti_{1-x-y}Al_xHf_yN$ films as a function of the Hf content of the used target, plotted within the TiN-AlN-HfN quasi-ternary phase diagram.

The chemical composition of the targets used as well as of the single-phase cubic coatings, which are used for further studies on their thermal stability, is shown in Tab. 5.1. It has to be mentioned that the chemical compositions of the films apply for both the powder (used for XRD) and the coated polycrystalline Al_2O_3 substrates (used for nanoindentation).

Table 5.1: Chemical composition of the single-phase cubic coatings used for further studies on the thermal stability.

Target System	Number of Ti platelets	Chemical composition [at%]				Coatings
		Ti	Al	Hf	N	
$Ti_{0.327}Al_{0.653}Hf_{0.02}$	6	19.50	30.77	0.88	48.84	$Ti_{0.381}Al_{0.602}Hf_{0.017}N$
$Ti_{0.317}Al_{0.633}Hf_{0.05}$	8	17.41	25.57	2.15	54.87	$Ti_{0.386}Al_{0.566}Hf_{0.048}N$
$Ti_{0.30}Al_{0.60}Hf_{0.10}$	6	18.32	28.99	4.96	47.73	$Ti_{0.350}Al_{0.555}Hf_{0.095}N$

5.1.5 Deposition rate

Figure 5.5 shows the thickness of the various Ti-Al-Hf-N coatings. The symbols are uniform with those in the ternary system of chapter 5.1.4, and show the structural development over the changing chemical composition. The open symbols represent the single-phase cubic structure and the half ones represent the cubic and wurtzite (c+w) mixed structure. As the deposition time was kept constant, it can be seen, that the thickness increases with increasing AlN content and the concomitant wurtzite phase fraction.

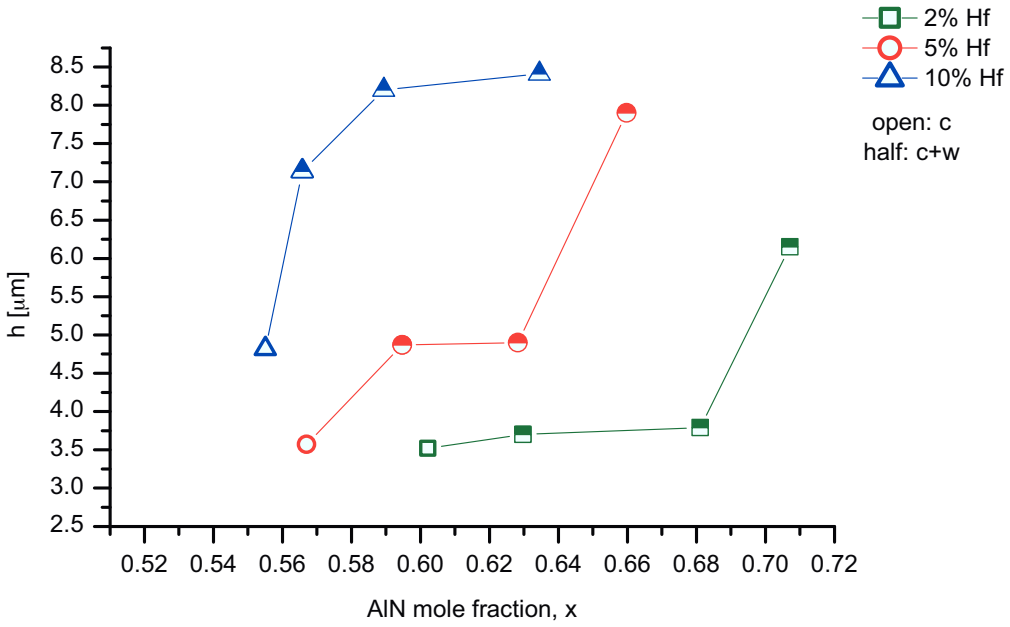

Figure 5.5: Coating thicknesses for the different $Ti_{1-x-y}Al_xHf_yN$ coatings as a function of their AlN mole fraction, x, prepared from the targets with 2, 5 and 10% Hf.

5.1.6 Residual stresses

Figure 5.6 shows that the compressive residual stresses of the various coatings decreases with increasing AlN content. The symbols here are again uniform to Fig. 5.4 and Fig. 5.5, so the structural change can be observed. The open symbols represent the single-phase cubic structure and the half ones represent the cubic and wurtzite (c+w) mixed structure. The decreasing residual stresses with increasing AlN

content can be explained by the concomitant increased fraction of wurtzite phases and the thereby decreasing grain size (indicating by the broadening of the XRD-peaks, see Figs. 5.1, 5.2 and 5.3).

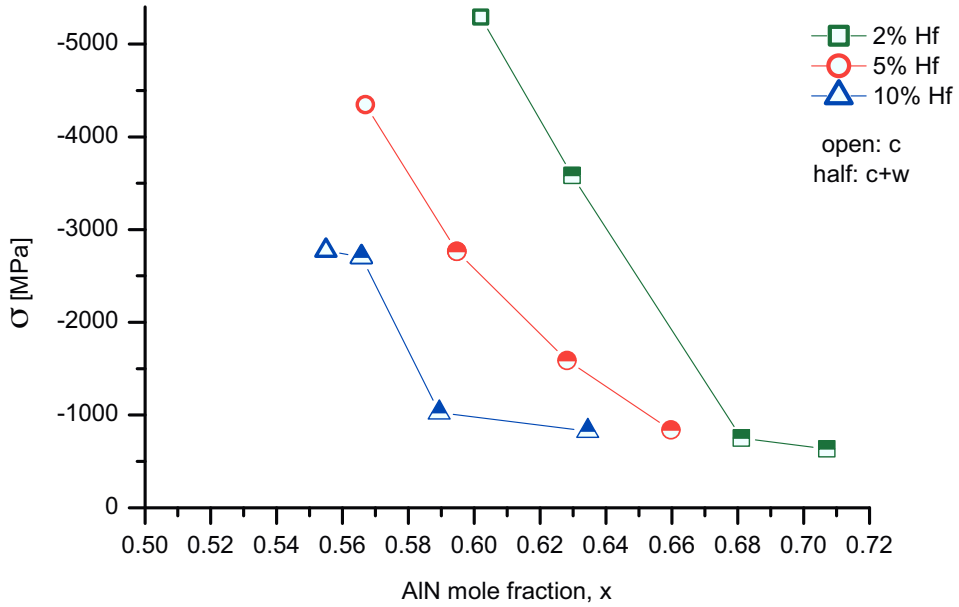

Figure 5.6: Residual stresses of the $Ti_{1-x-y}Al_xHf_yN$ coatings as a function of their AlN mole fraction, x, prepared from the targets with 2, 5 and 10% Hf.

5.2 Thermal stability of cubic stabilized Ti-Al-Hf-N coatings

Based on the previous studies, the thermal stability was investigated for the single-phase cubic $Ti_{0.381}Al_{0.602}Hf_{0.017}N$, $Ti_{0.386}Al_{0.566}Hf_{0.048}N$ and $Ti_{0.350}Al_{0.555}Hf_{0.095}N$ coatings. These show a fine fibrous structure in the as deposited state, with increasing column diameter with increasing Hf content, as can be seen from the SEM fracture cross section presented in Fig. 5.7a, b and c, respectively. The figure also shows that the coating thickness increases with increasing Hf content. Similar effects are observed for reactive sputtering of Al_2O_3, where the addition of W to the Al target results in an increasing sputter rate [49].

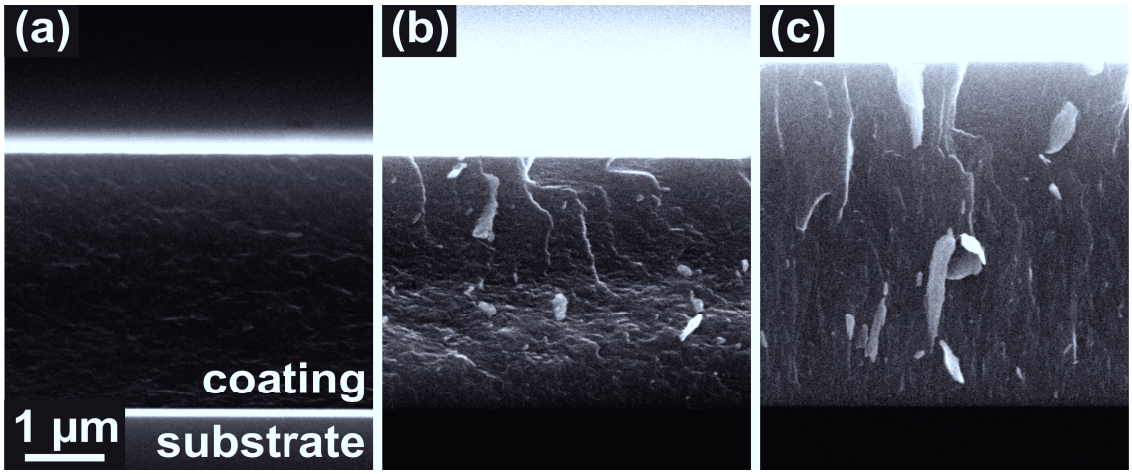

Figure 5.7: Cross-section SEM-images of as deposited (a) $Ti_{0.381}Al_{0.602}Hf_{0.017}N$, (b) $Ti_{0.386}Al_{0.566}Hf_{0.048}N$ and (c) $Ti_{0.350}Al_{0.555}Hf_{0.095}N$ coatings.

The hardness of the as deposited $Ti_{0.381}Al_{0.602}Hf_{0.017}N$, $Ti_{0.386}Al_{0.566}Hf_{0.048}N$ and $Ti_{0.350}Al_{0.555}Hf_{0.095}N$ coating is 37, 37 and 35 GPa, respectively. The biaxial compressive stresses are -5290, -4348 and -2772 MPa. Hence, the hardness and the compressive stresses decreases with increasing Hf content. As mentioned before the grain size increases with increasing Hf content, see Fig. 5.7. Consequently, the hardness reduction with increasing Hf can be explained by the reduction of compressive stresses and increasing grain size.

5.2.1 Structural changes with temperature

Figure 5.8 shows the structural development of the powdered coating $Ti_{0.381}Al_{0.602}Hf_{0.017}N$ with annealing temperature T_a in vacuum. With increasing T_a to

700 °C almost no change can be detected, even the width as well as the position of the XRD reflexes remain unchanged. For T_a = 800 °C, the matrix peak shifts to higher diffraction angels and also the width of the XRD peaks increases. Especially at the right-hand side of the peaks a shoulder starts to develop indicating the formation of Al-rich domains, in agreement to previous studies on Ti-Al-N based coatings. For T_a = 900 °C, the matrix peak further shifts towards c-AlN suggesting ongoing formation of Al-rich domains. With T_a = 1000 °C the matrix peak is almost completely gone and a broad reflex at the c-TiN position can be detected as well as at the position for w-AlN. With a further increase in T_a towards 1400 °C reflexes at the c-AlN position decrease in intensity, whereas those at w-AlN increase, suggesting the ongoing transformation from c-AlN to w-AlN. Also the reflexes at the position for c-TiN become sharper with increasing T_a. As no HfN can be detected, the results suggest that Hf prefers to stay within the TiN lattice and an ongoing transformation of the coating towards c-$Ti_{1-z}Hf_zN$ (z = y/(1-x) = 0.043) and w-AlN.

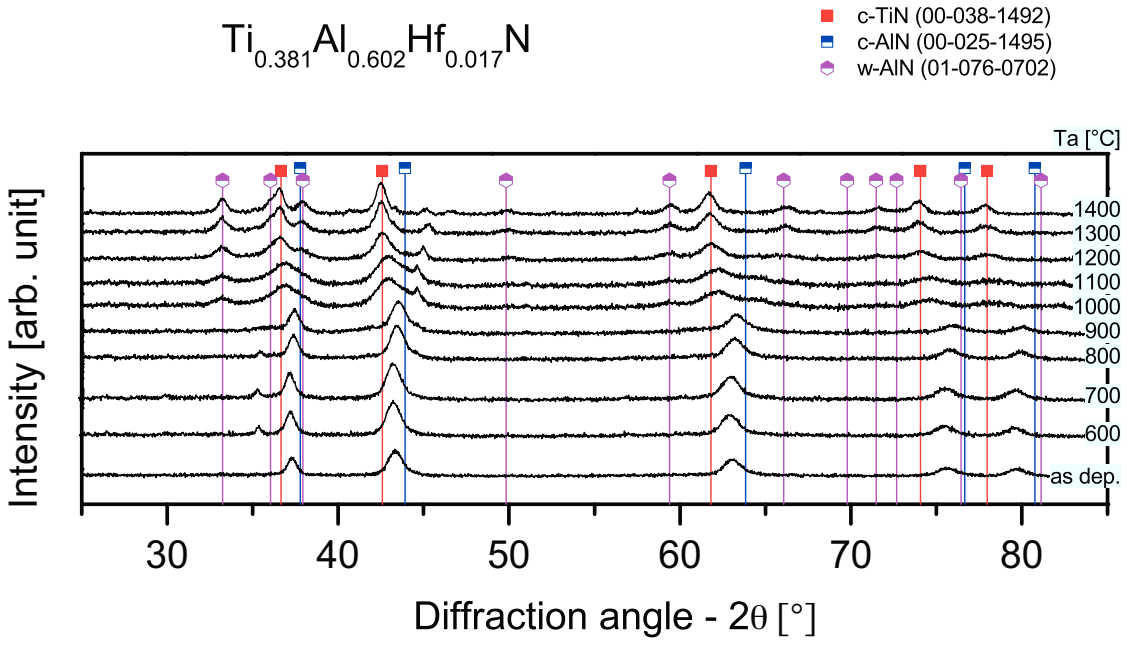

Figure 5.8: XRD patterns of $Ti_{0.381}Al_{0.602}Hf_{0.017}N$ coatings after annealing to 600 to 1400 °C.

A corresponding structural transformation from a single-phase cubic structure towards a film composed of w-AlN and c-$Ti_{1-z}Hf_zN$ with increasing T_a is obtained for the higher Hf containing film $Ti_{0.386}Al_{0.566}Hf_{0.048}N$, see Fig. 5.9.

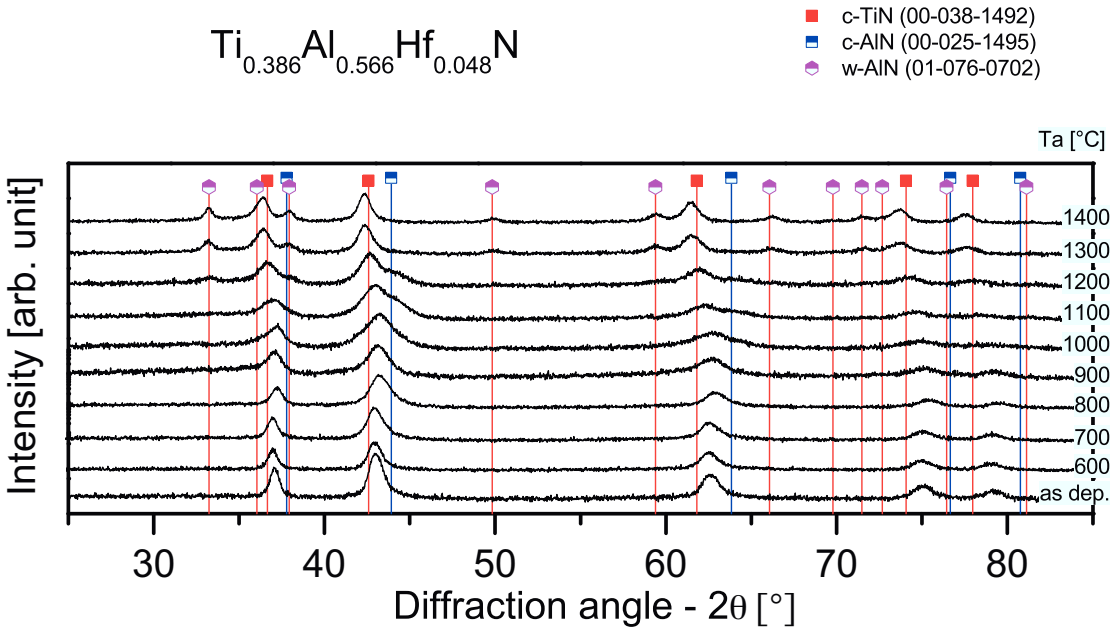

Figure 5.9: XRD patterns of $Ti_{0.386}Al_{0.566}Hf_{0.048}N$ coatings after annealing to 600 to 1400 °C.

Again up to T_a = 700 °C almost no change can be detected. For T_a = 800 °C the matrix peak boarders towards the position for c-AlN. At 1000 °C pronounced shoulders on both sides (Ti rich and Al rich) of the matrix develops which are available until 1100°C. For $T_a \geq$ 1200 °C w-AlN is detectable and almost no remaining matrix is present. Also here, no HfN can be detected whereas the cubic reflexes are at smaller diffraction angles as suggested for c-TiN, indicating the formation of a solid solution c-$Ti_{1-z}Hf_zN$ (with z = 0.111). For T_a = 1400 °C c-AlN reflexes decrease in intensity, whereby those of w-AlN increase.

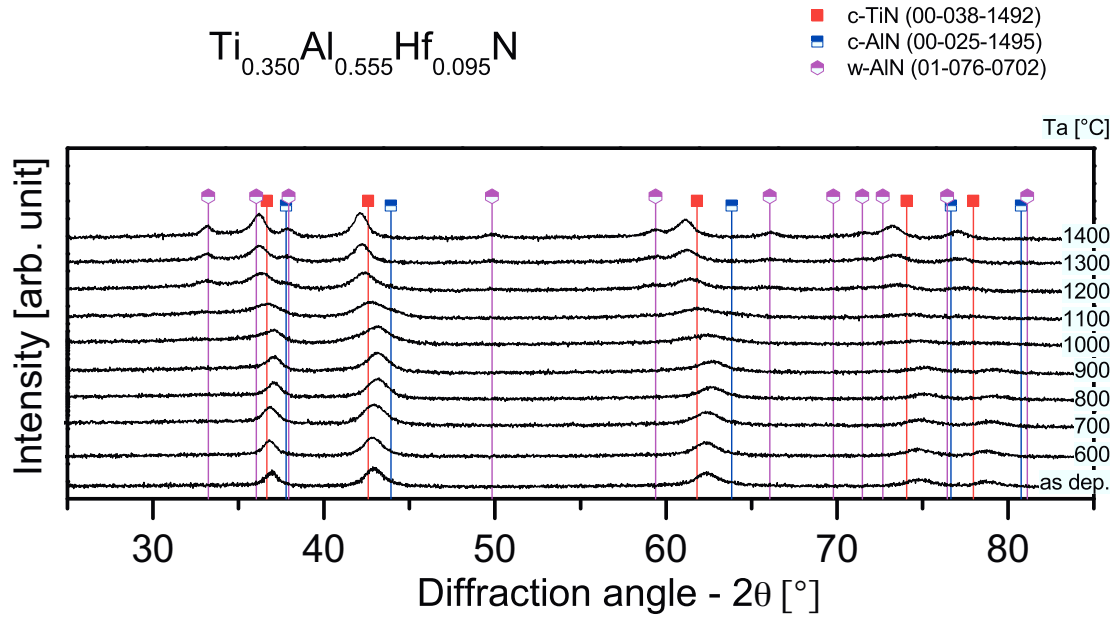

Figure 5.10: XRD patterns of $Ti_{0.350}Al_{0.555}Hf_{0.095}N$ coatings after annealing to 600 to 1400 °C.

The coating with the highest Hf content, $Ti_{0.350}Al_{0.555}Hf_{0.095}N$, shows a very comparable transformation from single-phase cubic towards a coating composed of w-AlN and c-$Ti_{1-z}Hf_zN$ (with z = 0.213). The pattern of these coating suggest a more nanocrystalline structure than the other ones. Again there is just c-$Ti_{1-z}Hf_zN$ and w-AlN for $T_a \geq 1200$ °C.

With increasing Hf content in the film, the position of the cubic reflexes, after a heat treatment to 1400 °C, shows and increasing deviation from c-TiN towards c-HfN. By the Cohen-Wagner method these patterns are analyzed. In the following chapters the determination of “stress-free” lattice parameters by this method is presented for the cubic phase of the $Ti_{0.381}Al_{0.602}Hf_{0.017}N$, $Ti_{0.386}Al_{0.566}Hf_{0.048}N$ and $Ti_{0.350}Al_{0.555}Hf_{0.095}N$ films in their as deposited state and after annealing to 1400 °C.

5.2.2 Lattice parameter

Table 5.2 shows the obtained specific parameter, for conducting the Cohen-Wagner analysis, which is described in chapter 4.5. These values were calculated from the cubic XRD reflex position of as deposited film powder, without annealing.

Table 5.2: Calculated values for the cubic lattice parameter at as deposited state, using the Cohen-Wagner method.

as deposited

$Ti_{0.381}Al_{0.602}Hf_{0.017}N$								
2θ [°]	**θ [°]**	**d [Å]**	**h**	**k**	**l**	**a [Å]**	**Cohen-Wagner parameter**	**$a_{Cohen-Wagner}$ [Å]**
37.4	18.7	2.401649411	1	1	1	4.159778802	0.049417982	**4.1575**
43.44	21.72	2.08068146	2	0	0	4.16136292	0.055456389	
63.17	31.585	1.470130837	2	2	0	4.158157936	0.069114611	
75.65	37.825	1.255601766	3	1	1	4.164359945	0.072307667	
79.75	39.875	1.201032892	2	2	2	4.16049998	0.072383585	
$Ti_{0.386}Al_{0.566}Hf_{0.048}N$								
2θ [°]	**θ [°]**	**d [Å]**	**h**	**k**	**l**	**a [Å]**	**Cohen-Wagner parameter**	**$a_{Cohen-Wagner}$ [Å]**
37.22	18.61	2.412849738	1	1	1	4.179178337	0.049226396	**4.1778**
43.16	21.58	2.093529223	2	0	0	4.187058445	0.055193866	
62.75	31.375	1.47895708	2	2	0	4.183122323	0.068930595	
75.22	37.61	1.261708832	3	1	1	4.184614789	0.072271731	
79.22	39.61	1.207732386	2	2	2	4.183707709	0.072400902	
$Ti_{0.350}Al_{0.555}Hf_{0.095}N$								
2θ [°]	**θ [°]**	**d [Å]**	**h**	**k**	**l**	**a [Å]**	**Cohen-Wagner parameter**	**$a_{Cohen-Wagner}$ [Å]**
36.95	18.475	2.429858797	1	1	1	4.208638891	0.048937811	**4.2273**
42.95	21.475	2.103277936	2	0	0	4.206555872	0.054995826	
62.37	31.185	1.48705186	2	2	0	4.206017816	0.068759892	
74.92	37.46	1.266015475	3	1	1	4.198898309	0.072243512	
78.89	39.445	1.211954809	2	2	2	4.19833461	0.072407621	

Figure 5.11 shows the particular trend lines, using the Cohen-Wagner method, to obtain the ascertained Cohen-Wagner lattice parameter, written in table 5.2.

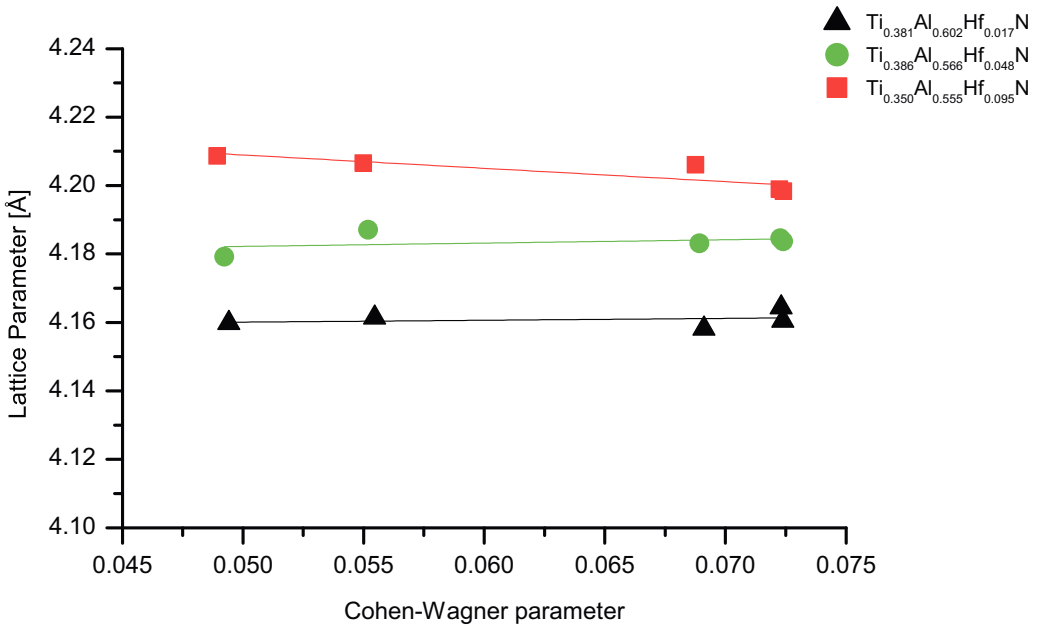

Figure 5.11: Lattice parameter for as deposited c-$Ti_{1-x-y}Al_xHf_yN$ coatings as a function of the Cohen-Wagner parameter ($cos^2(\theta)/(sin(\theta))-cos^2(\theta)/\theta$).

Figure 5.12 shows the obtained lattice parameters of the single-phase cubic $Ti_{0.381}Al_{0.602}Hf_{0.017}N$, $Ti_{0.386}Al_{0.566}Hf_{0.048}N$ and $Ti_{0.350}Al_{0.555}Hf_{0.095}N$ coatings as a function of their Hf content y.

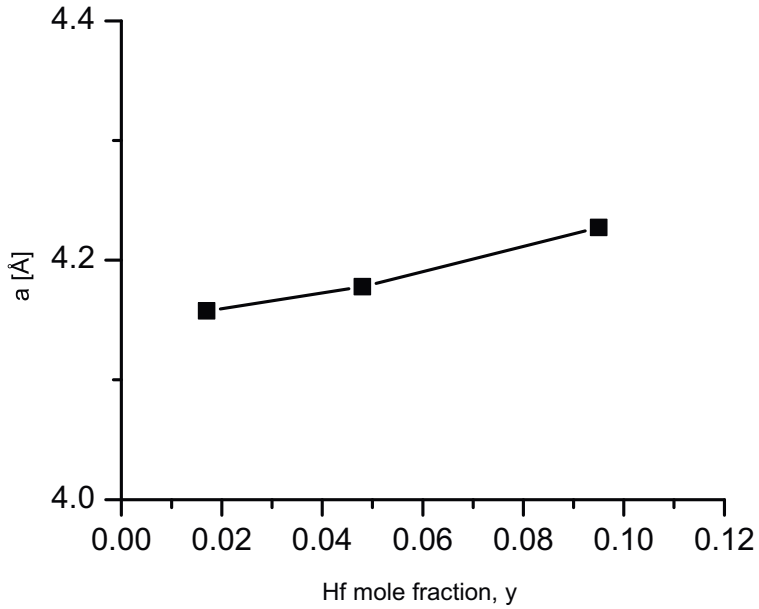

Figure 5.12: The lattice parameter a for the as deposited c-$Ti_{1-x-y}Al_xHf_yN$ films as a function of their HfN mole fraction, y.

Table 5.3 shows the same calculations as above but for the cubic phase after annealing the films to 1400 °C [50].

Table 5.3: Calculated values for the lattice parameter of the cubic phases (i.e., $Ti_{0.957}Hf_{0.043}N$, $Ti_{0.889}Hf_{0.111}N$ and $Ti_{0.787}Hf_{0.213}N$) of the coatings $Ti_{0.381}Al_{0.602}Hf_{0.017}N$, $Ti_{0.386}Al_{0.566}Hf_{0.048}N$ and $Ti_{0.350}Al_{0.555}Hf_{0.095}N$ after annealing to 1400°C, using the Cohen-Wagner method.

T_a = 1400 °C								
$Ti_{0.957}Hf_{0.043}N$								
2θ [°]	**θ [°]**	**d [Å]**	**h**	**k**	**l**	**a [Å]**	**Cohen-Wagner parameter**	**$a_{Cohen-Wagner}$ [Å]**
36.56	18.28	2.454879437	1	1	1	4.251975911	0.048518422	**4.2625**
42.52	21.26	2.123548031	2	0	0	4.247096062	0.054587263	
61.71	30.855	1.5013634	2	2	0	4.246496966	0.068453923	
73.96	36.98	1.280055942	3	1	1	4.24546527	0.072135823	
77.88	38.94	1.225127094	2	2	2	4.243964746	0.072408793	
$Ti_{0.889}Hf_{0.111}N$								
2θ [°]	**θ [°]**	**d [Å]**	**h**	**k**	**l**	**a [Å]**	**Cohen-Wagner parameter**	**$a_{Cohen-Wagner}$ [Å]**
36.41	18.205	2.464648159	1	1	1	4.268895834	0.048356323	**4.2852**
42.35	21.175	2.131678294	2	0	0	4.263356587	0.054424611	
61.46	30.73	1.506869764	2	2	0	4.262071314	0.06833489	
73.71	36.855	1.283778442	3	1	1	4.257811406	0.072103431	
77.55	38.775	1.229514018	2	2	2	4.259161497	0.072402833	
$Ti_{0.787}Hf_{0.213}N$								
2θ [°]	**θ [°]**	**d [Å]**	**h**	**k**	**l**	**a [Å]**	**Cohen-Wagner parameter**	**$a_{Cohen-Wagner}$ [Å]**
36.2	18.1	2.478462885	1	1	1	4.292823641	0.048128647	**4.3117**
42.11	21.055	2.143270942	2	0	0	4.286541884	0.054193904	
61.14	30.57	1.513987685	2	2	0	4.282203836	0.068180021	
73.26	36.63	1.290549338	3	1	1	4.280267927	0.072040601	
77.05	38.525	1.236240692	2	2	2	4.282463378	0.072387845	

Figure 5.13 shows the particular trend lines, using the Cohen-Wagner method, to obtain the ascertained Cohen-Wagner lattice parameter, written in table 5.3.

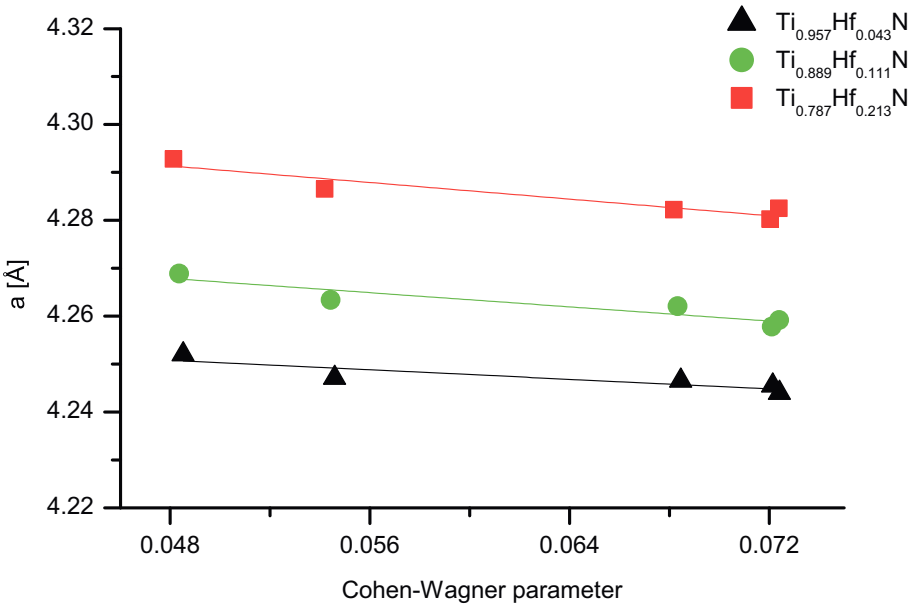

Figure 5.13: Lattice parameter a for the phases c-$Ti_{0.957}Hf_{0.043}N$, c-$Ti_{0.889}Hf_{0.111}N$ and c-$Ti_{0.787}Hf_{0.213}N$ as a function of the Cohen-Wagner parameter ($\cos^2(\theta)/(\sin(\theta))-\cos^2(\theta)/\theta$), after annealing the respective coatings to 1400 °C.

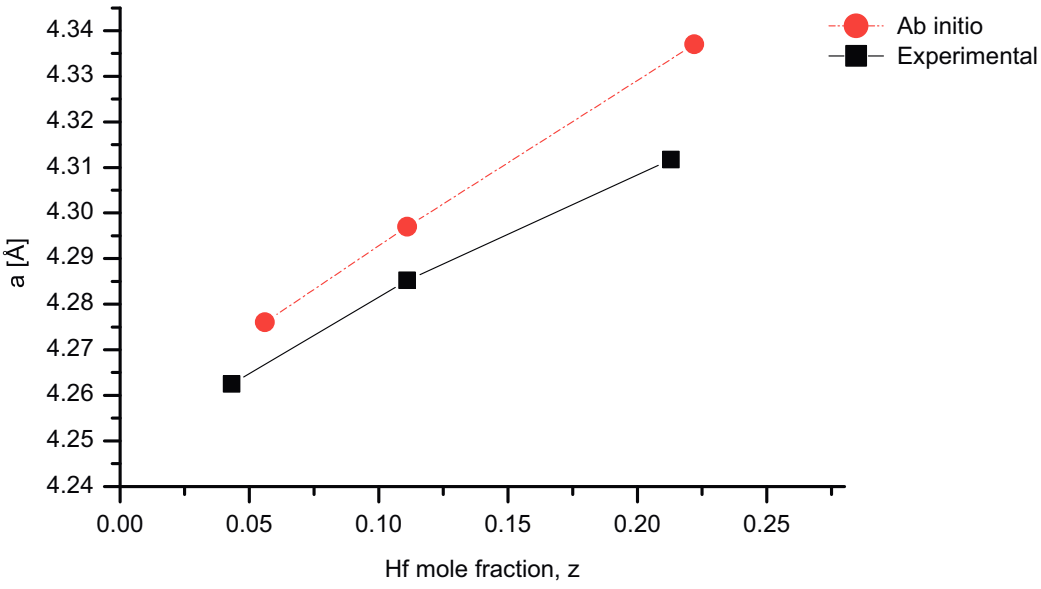

Figure 5.14: The lattice parameter a for the cubic phases $Ti_{1-z}Hf_zN$ of the respective films, after annealing to 1400°C and the ab initio obtained lattice parameters for c-$Ti_{1-z}Hf_zN$, as a function of their HfN mole fraction z.

As mentioned in the previous chapters, if the Hf content of the coating is normalized to the Ti content, as the XRD results show that a c-$Ti_{1-z}Hf_zN$ is formed, rather than a separate c-TiN and c-HfN, the coatings $Ti_{0.381}Al_{0.602}Hf_{0.017}N$, $Ti_{0.386}Al_{0.566}Hf_{0.048}N$ and $Ti_{0.350}Al_{0.555}Hf_{0.095}N$ should contained the phase w-AlN and $Ti_{0.957}Hf_{0.043}N$, $Ti_{0.889}Hf_{0.111}N$ and $Ti_{0.787}Hf_{0.213}N$, respectively, after annealing to 1400°C.
Additional to the calculation with the Cohen-Wagner method, calculations with ab initio were done [50]. Figure 5.14 shows the experimentally obtained lattice parameters a for the phases $Ti_{0.957}Hf_{0.043}N$, $Ti_{0.889}Hf_{0.111}N$ and $Ti_{0.787}Hf_{0.213}N$ as a function of their HfN mole fraction z. Furthermore, the figure shows the ab initio obtained lattice parameters for c-$Ti_{0.944}Hf_{0.056}N$, c-$Ti_{0.889}Hf_{0.111}N$ and c-$Ti_{0.778}Hf_{0.222}N$ as a function of their HfN mole fraction z. The difference between the calculated and measured lattice parameters are with 0.5% really small and the trend is also the same. The chemical compositions used in the ab initio calculations is a little bit different.

5.2.3 Coating thickness

Figure 5.15 shows the coating thicknesses of $Ti_{0.381}Al_{0.602}Hf_{0.017}N$, $Ti_{0.386}Al_{0.566}Hf_{0.048}N$ and $Ti_{0.350}Al_{0.555}Hf_{0.095}N$ over the annealing temperature. Especially the low Hf containing film, $Ti_{0.381}Al_{0.602}Hf_{0.017}N$, shows a pronounced increase in thickness when annealed to 1100 °C. This is also the temperature where w-AlN formation can be detected. Consequently, the increasing thickness is related to the formation of the wutzite phase, which is connected with an increase of the specific volume (w-AlN has an around 28% larger volume than c-AlN).

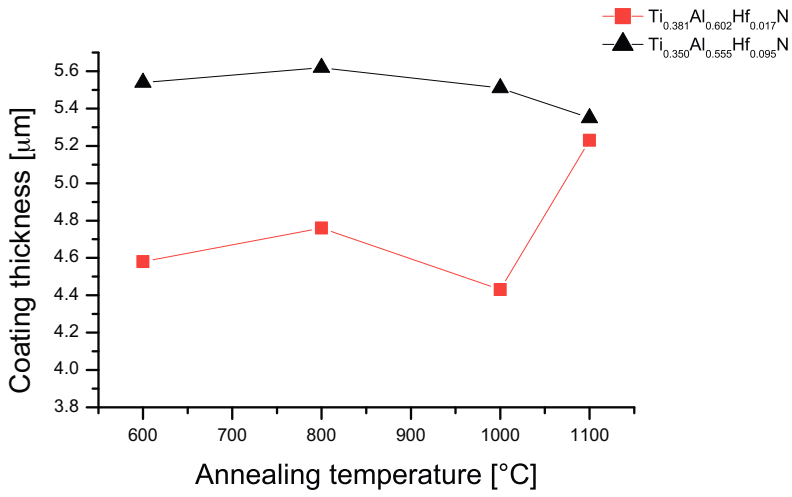

Figure 5.15: Coating thickness over the annealing temperature for the c-$Ti_{1-x-y}Al_xHf_yN$ coatings.

5.2.4 Mechanical properties

Hardness measurements were carried out using a nanoindenter equipped with a Berkovich tip. Figure 5.16 shows the hardness over the temperature for the coatings $Ti_{0.381}Al_{0.602}Hf_{0.017}N$, $Ti_{0.386}Al_{0.566}Hf_{0.048}N$ and $Ti_{0.350}Al_{0.555}Hf_{0.095}N$, which are single-phase cubic in their as deposited state. For comparison the H vs. T_a curve of $Ti_{0.40}Al_{0.60}N$ is added. This coating exhibits the lowest hardness values in the as deposited state and over the whole annealing range. By introducing Hf to the coating the hardness increases from around 30 GPa to 36 GPa.

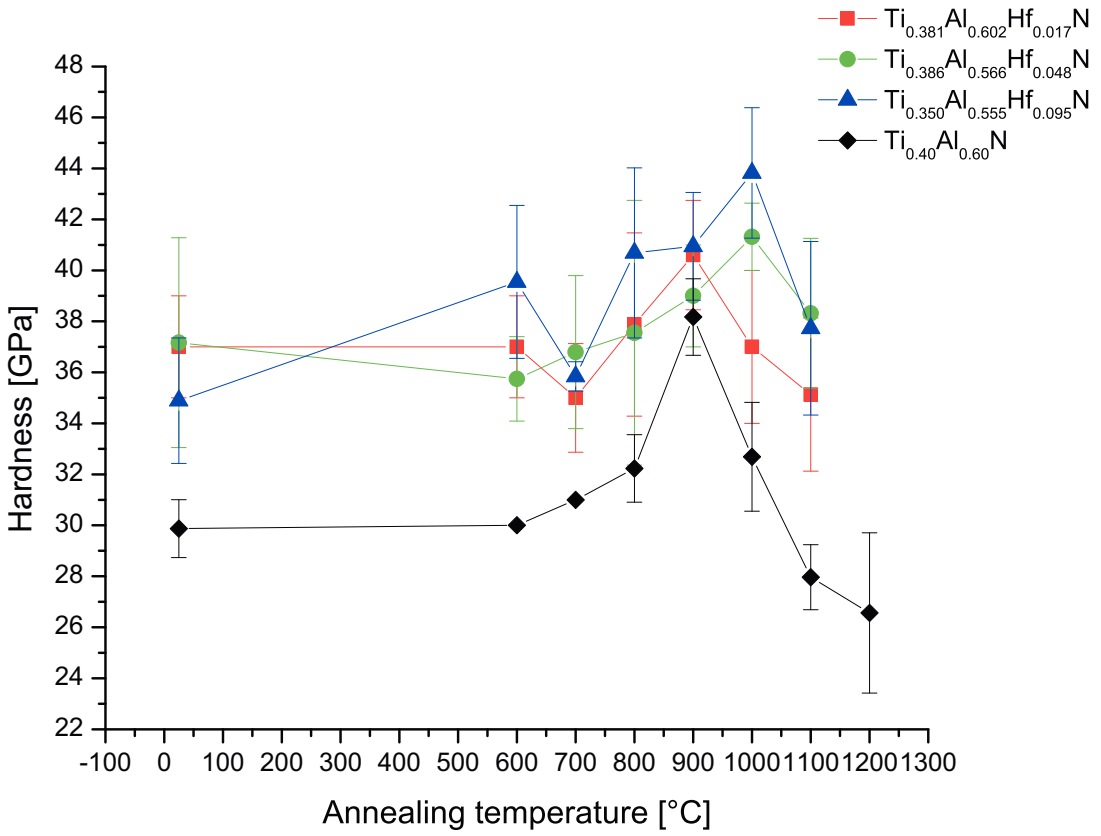

Figure 5.16: Hardness over annealing temperature T_a for various $Ti_{1-x-y}Al_xHf_yN$ coatings.

With increasen T_a up to 900 °C the hardness increases for all coatings investigated as their supersaturated cubic $Ti_{1-x-y}Al_xHf_yN$ phase spinodal decomposes to form cubic Al-rich and Ti-rich domains, see chapter 5.1 and Figs. 5.1, 5.2 and 5.3. A further increase in T_a to 1000 °C results in a hardness reduction for the Hf-free and Hf-poor coatings $Ti_{0.40}Al_{0.60}N$ and $Ti_{0.381}Al_{0.602}Hf_{0.017}N$. This is also the temperature where w-AlN formation can be detected for these coatings. The higher Hf containing films $Ti_{0.386}Al_{0.566}Hf_{0.048}N$ and $Ti_{0.350}Al_{0.555}Hf_{0.095}N$ reach their peak hardness values of 41.3

and 43.8 GPa with annealing to T_a = 1000 °C. Further increasing T_a 1100°C results in a hardness reduction but still have values of around 38 GPa. Also the lower Hf-containing film still exhibits only around 28 GPa. Based on these investigations it can be concluded that Hf shifts the peak hardness to higher values (from 38.2 to 40.6 GPa to 41.3 to 43.8 GPa) and higher temperatures (from 900 °C to 1000 °C), and also the hardness-reduction retarded, as the formation of w-AlN is retarded.

6 Summary and conclusion

The aim of this thesis was to prepare (by means of the PVD technique of reactive magnetron sputtering) and investigate single-phase cubic Ti-Al-Hf-N coatings. For the deposition of various Hf-containing films three different Ti-Al-Hf targets, all with an Al/Ti ratio of 2, with 2, 5 and 10 at% Hf were used.

Further chemical variation of the coatings was obtained by placing up to 8 Ti platelets at the sputter race-track of the individual targets. Thereby, also the Ti content of the films could be adjusted and consequently their structure. Without the addition of Ti platelets to the target, all films deposited were predominant wurtzite structured. By the addition of Ti to the targets the structure of the films gradually changed towards cubic. Adding 6, 8 and 6 Ti platelets to the $Ti_{0.327}Al_{0.653}Hf_{0.02}$, $Ti_{0.317}Al_{0.633}Hf_{0.05}$ and $Ti_{0.30}Al_{0.60}Hf_{0.10}$ targets leads to the deposition of single-phase cubic $Ti_{0.381}Al_{0.602}Hf_{0.017}N$, $Ti_{0.386}Al_{0.566}Hf_{0.048}N$ and $Ti_{0.350}Al_{0.555}Hf_{0.095}N$ coatings, respectively . The hardness of these coatings decrease with increasing Hf content from ~37 to 35 GPa. This can be attributed to decreasing compressive stresses from -5.3 to -2.8 GPa and increasing grain size with increasing Hf content. For studying their thermal stability, these single-phase cubic films were deposited onto low-alloy steel and polycrystalline Al_2O_3 substrates. The low-alloy steel foil was chemically removed after deposition to obtain free-standing film-powder, which was used for structural investigations by XRD, in the as-deposited state and after vacuum annealing up to 1400 °C. Films on polycrystalline Al_2O_3 substrates were used for nanoindentation measurements, in their as-deposited state and after vacuum annealing to temperatures between 600 and 1100 °C (step size 100 °C).

The as-deposited single-phase cubic $Ti_{0.381}Al_{0.602}Hf_{0.017}N$, $Ti_{0.386}Al_{0.566}Hf_{0.048}N$ and $Ti_{0.350}Al_{0.555}Hf_{0.095}N$ coatings exhibit a lattice parameter a of 4.16, 4.18 and 4.22 Å, respectively. With increasing the annealing temperature T_a to 900 °C, all films exhibit a broadening of their cubic matrix XRD reflexes and the formation of shoulders (on both sides) of these reflexes. This suggests the formation of Al-rich and Ti-rich cubic domains, which is more pronounced for the films with higher Hf content. Already after annealing at T_a = 1000 °C wurtzite structure AlN (w-AlN) can be detected for the low Hf containing film $Ti_{0.381}Al_{0.602}Hf_{0.017}N$. The higher Hf containing films, $Ti_{0.386}Al_{0.566}Hf_{0.048}N$ and $Ti_{0.350}Al_{0.555}Hf_{0.095}N$, exhibit the formation of w-AlN only after annealing at $T_a \geq 1200$ °C. Based on these investigations, it can be concluded, that Hf promotes the separation of the supersaturated cubic $Ti_{1-x-y}Al_xHf_yN$ phase to form cubic Al-rich and Ti-rich domains, but retards the formation of the stable w-AlN

phase. After annealing to T_a = 1400 °C, all films investigated exhibit one wurtzite phase, w-AlN, and one cubic phase. The latter shows a shift of the XRD peaks from c-TiN towards c-HfN with increasing Hf content. Consequently, the cubic phase can be assigned to c-$Ti_{1-z}Hf_zN$, with z = y/(1-x). Based on these investigations, the lattice parameters of the formed cubic solid solution $Ti_{0.96}Hf_{0.04}N$, $Ti_{0.89}Hf_{0.11}N$ and $Ti_{0.79}Hf_{0.21}N$ phases are 4.26, 4.29 and 4.31Å, respectively. The structural changes with annealing temperature cause also changes in the film hardness.

With increasing T_a up to 900 °C the hardness increases for all coatings investigated as their supersaturated cubic $Ti_{1-x-y}Al_xHf_yN$ phase decomposes to form cubic Al-rich and Ti-rich domains. While a further increase of T_a to 1000 °C results in a reduction of the hardness for $Ti_{0.381}Al_{0.602}Hf_{0.017}N$ from its peak value of 40.6 GPa to 37.0 GPa, the hardness of the higher Hf containing films $Ti_{0.386}Al_{0.566}Hf_{0.048}N$ and $Ti_{0.350}Al_{0.555}Hf_{0.095}N$ further increases to their peak value of 41.3 and 43.8 GPa, respectively. Even after annealing at 1100 °C their hardness is at the high level of ~38 GPa. This is in agreement to the structural development of the coatings, which exhibits the formation of w-AlN in $Ti_{0.381}Al_{0.602}Hf_{0.017}N$ already after annealing at T_a = 1000 °C but in $Ti_{0.386}Al_{0.566}Hf_{0.048}N$ and $Ti_{0.350}Al_{0.555}Hf_{0.095}N$ only after annealing at T_a ≥ 1200 °C.

Based on the results presented it can be concluded, that Hf promotes the formation of cubic Al-rich and Ti-rich domains during annealing but retards the formation of the stable phase w-AlN. Consequently, Hf has a pronounced 'age-hardening' combined with a retarded 'over-aging' effect on Ti-Al-N based coatings.

References

[1] Ohring M., The material science of thin films, Academic Press (2002).

[2] Kutschej K., et al., Surface and Coatings Technology 200 (2005) 113-117.

[3] PalDey S., S.C. Deevi, Materials Science and Engineering, A342 (2003) 58-79.

[4] Bunshah R.F., D.M. Mattox, Deposition Technologies for Films and Coatings, Development and Applications, Noyes Publications, New Jersey (1982).

[5] Haefer R.A., Oberflächen und Dünnschicht-Technologie, Teil I, Springer Verlag (1987).

[6] Mattox Donald M., Physical Vapor Deposition (PVD) Processing, Elsevier, UK (2010).

[7] Rovere F., Theoretical and experimental assessment of Cr-Al-Y-N as protective coating for y-TiAl based alloys, Shaker Verlag GmbH, Germany (2010).

[8] Smith Donald L., Thin film depositions, principles and practice, McGraw-Hill, (1995).

[9] Frey H., Vakuumbeschichtung 1, Plasmaphysik - Plasmadiagnostik - Analytik, VDI Verlag, Berlin (1995).

[10] Green J. E., Handbook of crystal growth, Elsevier (1993)

[11] Green J. E., Bunshah, Handbook of deposition technologies for films and coatings, Noyes Publications, Park Ridge (1994), p.681.

[12] Konuma M., Film deposition by plasma techniques, Springer Verlag (1992).

[13] Adibi F., et al., Journal of Applied Physics 73/12 (1993) 8580.

[14] Petrov I., et al., Journal of Vacuum Science and Technology A: Vacuum, Surfaces and Films 21/5 (2003).

[15] Mayrhofer P. H., PhD Thesis, Institute of Physical Metallurgy and Materials Testing, University of Leoben, Leoben, 2001.

[16] Moser M., PhD Thesis, Institute of Physical Metallurgy and Materials Testing, University of Leoben, Leoben, 2008.

[17] Barna P. B., Academik M 1998, Thin Solid Films 317, 27.

[18] Messier R., Giri A. P., Roy R. A. 1984, Journal of Vacuum Science & Technology A: Vacuum, Surfaces, and Films 2, 500.

[19] A. Anders, Thin Solid Films 518 (2010) 4087–4090

[20] Knotek O., M. Böhmer, Journal Vacuum Science Technology A4, (1984).

[21] Chaleix-Combadiere L., Machet J., Vide: Science, Technique et Applications, 1996, p.116.

[22] Hasegawa H., et al., Surface and Coatings Technology 132/1 (2000) 76.

[23] Jehn H. A., et al., J.Vac.Sci.Tech.A. 4/6, Nov.-Dec. 1986 (1986) 2701.

[24] Miura Y., Fujieda S., Journal of Applied Physics 81/9 (1997) 6476.

[25] Mayrhofer P. H., et al., Advanced Engineering Materials 7/12 (2005) 1071-1082.

[26] Mayrhofer P. H., et al., Applied Phyics Letter 83/10 (2003) 2049 – 2051.

[27] Schuster J. C., Bauer J. , Journal of Solid State Chemistry, (1984).

[28] Jeitschko et al., Monatsh. Chem, (1963).

[29] Holleck H., Surface and Coating Technologie Vol. 36, 151 (1988).

[30] Porter D. A., Easterling K. E., Phase Transformation in Metals and Alloys, 2nd Edition, Chapman & Hall (1992).

[31] Pock M., Diploma Thesis, Institute of Physical Metallurgy and Materials Testing, University of Leoben, Leoben, 2004.

[32] Taniguchi S., et al., Oxidation of Metals Vol. 42, Nos. 3/4 (1994) 205-222.

[33] Cui C. Y., et al.,Journal of Alloys and Compounds 463 (2008) 263 – 270.

[34] Zheng P., et al., Materials Science and Engineering A 483-484 (2008) 656-659.

[35] User Manual A400 VL, Leybold AG.

[36] Operational Manual ACG-6B, ENI Company Ltd.

[37] User Guide Tylan General R 7030/7031, Tylan General GmbH.

[38] User Guide Leybold Vacuum, Leybold AG.

[39] User Manual Duo 20, Pfeiffer Vacuum GmbH (2002).

[40] Allmann R., Röngten-Pulverdiffractometrie: Rechnergeschützte Auswertung, Phasenanalyse und Strukturbestimmung, Berlin, Springer (2003).

[41] Cullity B. B., Stock S. R. Elements of X-ray diffraction, New Jersey, Prentice Hall (2001).

[42] Klug H. P., Alexander L. E. X-Ray Diffraction Procedures, New York, John Wiley & Sons (1974).

[43] Fischer-Cripps A. C., Nanoindentation, New York, Springer Science + Business Media (2004).

[44] Chudoba T., In: Cavaleiro A., De Hosson J. T. M., editors. Nanostructured Coatings, New York, Springer (2006).

[45] Oliver W. C., Pharr G. M., 1992 Journal of Materials Research 7, 1564.

[46] User Manual HTM Reetz GmbH – Vakuum – Kaltwandofen.

[47] Wagner C. N. J., Local Atomic Arrangements Studied by X-ray Diffraction, Gordon and Breach, New York, 1966.

[48] Evans B., Wilson J., Encyclopedia of materials characterization, Butterworth-Heinemann (1992).

[49] Kubart T., et al., Surface & Coatings Technology 204 (2010) 3882–3886

[50] Holec D., Department of Physical Metallurgy and Materials Testing, University of Leoben.